https://doi.org/10.1016/j.ejor.2018.12.020

A Strengthened Mixed-Integer Linear Programming Formulation for Combined-Cycle Units*

Lei Fan[a], **Kai Pan**[b†], and **Yongpei Guan**[c]

[a]Siemens Energy Management, Minnetonka, MN 55305, USA, eefanlei@gmail.com

[b]Department of Logistics and Maritime Studies,
The Hong Kong Polytechnic University, Kowloon, Hong Kong, kai.pan@polyu.edu.hk

[c]Department of Industrial and Systems Engineering,
University of Florida, Gainesville, FL 32611, USA, guan@ise.ufl.edu

Abstract

Due to increased utilization of gas-fired combined-cycle units for electric power generation in the U.S., accurate and computationally efficient models for operating these units are crucial to keep an electricity system reliable. The recently proposed edge-based formulation for combined-cycle units helps accurately describe the operations of combined-cycle units by capturing the state transition processes and physical constraints for each turbine. In this paper, we derive tighter constraints and several families of strong valid inequalities to strengthen the edge-based model and improve its computational efficiency by exploring the physical characteristics of combined-cycle units and utilizing the edge-based modeling framework. Meanwhile, we provide the validity and facet-defining proofs for certain inequalities. Finally, the computational results indicate that our derived formulation significantly reduces the computational time, which verifies the effectiveness of proposed tighter constraints and strong valid inequalities.

Key words: OR in Energy, Combined-Cycle Units, Unit Commitment, Strong Valid Inequalities, Strong Mixed-Integer Linear Programming (MILP) Formulation.

*Earlier versions are available online at http://www.optimization-online.org/DB_HTML/2016/08/5574.html and in the first author's Ph.D. dissertation [11] at https://search.proquest.com/docview/1786690481?pq-origsite=gscholar.

†Corresponding author

1 Introduction

Several factors such as fuel prices, environmental regulations, flexibility, and energy policies increase the dependence of U.S. power generation on electricity generators using natural gas. For instance, in Midcontinent ISO[1] (MISO), natural gas combined-cycle units are planned for its future electric generation capacity expansions [19]. As the share of combined-cycle units in ISOs' generation portfolio (including thermal, hydro, pumped-storage hydro generators, etc.) increases, U.S. ISOs have started to improve the mathematical model of combined-cycle units in their unit commitment (UC) models [31] so that the new model can better take advantage of the capability of the combined-cycle units.

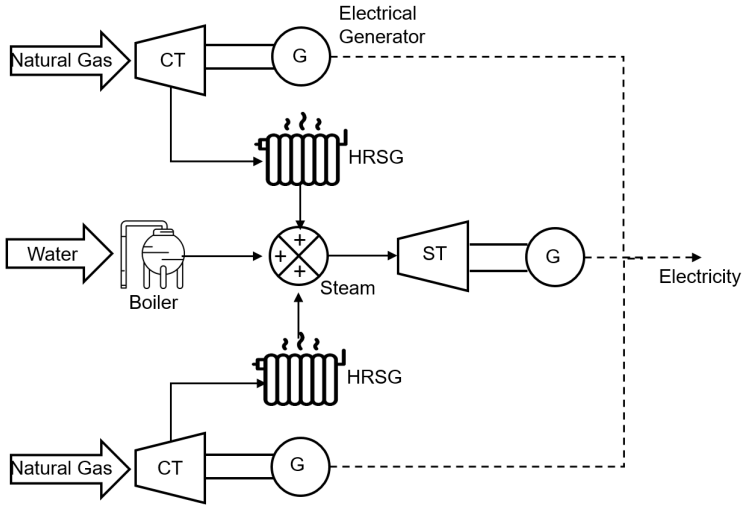

Figure 1: Combined-Cycle Unit

A combined-cycle unit usually consists of one or more combustion turbines (CTs) using natural gas, each linked to a heat recovery steam generator (HRSG), and one or more steam turbines (STs) driven by the steam produced from HRSG(s) (and possibly one more boiler) [4]. For example, Fig. 1 shows a combined-cycle unit with two CTs, two HRSGs, one ST, and one boiler that improves the steam pressure. Each combustion and steam turbine connects to an electrical generator so that a turbine can drive a generator to produce electricity. In terms of how many turbines (and thereby electrical generators) are committed (or called "online") to produce electricity, the whole combined-cycle unit can be operated at different modes (or called "configurations" or "states"), with each mode corresponding to committing a subset of CTs and STs online. Note that we

[1] An ISO, i.e., Independent System Operator, in the U.S. is an electric power transmission system operator which coordinates, controls, and monitors the electric grid in a certain region.

interchangeably use "mode", "configuration", and "state" in this paper. Accordingly, a state transition (i.e., from one mode to another mode) can be performed by starting up or shutting down a turbine. This basic infrastructure makes the combined-cycle unit very popular because of its high efficiency, fast response, shorter installation time, and environmental friendliness. For instance, it enables the combined-cycle unit to hedge against the uncertainty cuased mainly by renewable generations, while in both the U.S. and Europe [3], the proportion of renewables in their generation portfolios has increased significantly in the past years. In spite of such increasing popularity and importance, the intrinsically complex physical characteristics of each individual turbine and the whole combined-cycle unit create a difficult task when operating the combined-cycle unit. When further incorporating the combined-cycle units into traditional thermal unit commitment problems (e.g., [10, 16, 28, 29]), U.S. ISOs face two significant challenges: (1) deriving an accurate model to guarantee the feasibility of combined-cycle unit operations and (2) improving the computational efficiency so that the unit commitment solutions can be obtained within a given timeline. A good mathematical model for operating combined-cycle units is expected to accurately describe the operations of the whole combined-cycle unit. However, a more accurate model is usually more complicated, meaning heavier computational burden. Accordingly, it is very challenging to achieve a satisfactory computational performance when the accurate model of combined-cycle units is included in the traditional thermal unit commitment model.

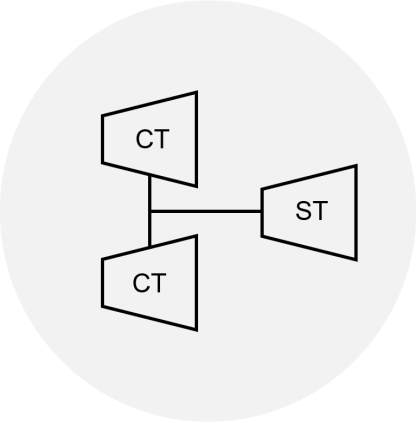

Figure 2: Aggregated model

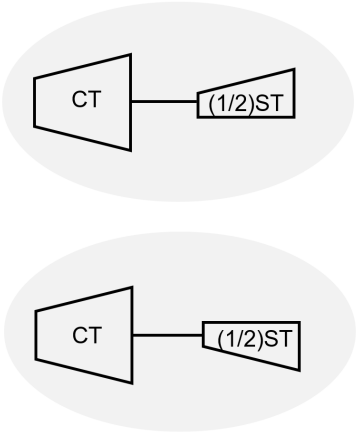

Figure 3: Pseudo unit model

To solve this problem, in most circumstances of current practices, U.S. ISOs reduce the computational burden by sacrificing the accuracy of the combined-cycle unit model. For instance, there are two modeling approaches initially used in practice: 1) aggregated model and 2) pseudo unit model. An aggregated model simply uses a single traditional thermal unit to represent the whole

combined-cycle unit by ignoring the relationships among CTs and STs. A pseudo unit model associates each CT with a portion of ST by dividing the whole combined-cycle unit into several small units. By taking the combined-cycle unit in Fig. 1 as an example, its corresponding aggregated model representing a single aggregated unit is shown in Fig. 2 and the pseudo unit model representing two small pseudo units is shown in Fig. 3. Each pseudo unit in Fig. 3 associates one CT together with a half of ST. As a result, these less accurate models bring challenges to the feasibility of operations, leading to the so-called feasibility issue in practice. For example, prohibited combinations of CTs and STs may appear in the optimal solutions obtained by the aggregated model and pseudo unit model approaches. Therefore, some ISOs developed the third modeling approach, i.e., configuration-based model (see, e.g., the early work in [18] for the corresponding mixed-integer linear programming [MILP] formulation), which considers each configuration as an independent unit. For instance, five possible configurations for a combined-cycle unit with 2CTs and 1ST are shown in Fig. 4.

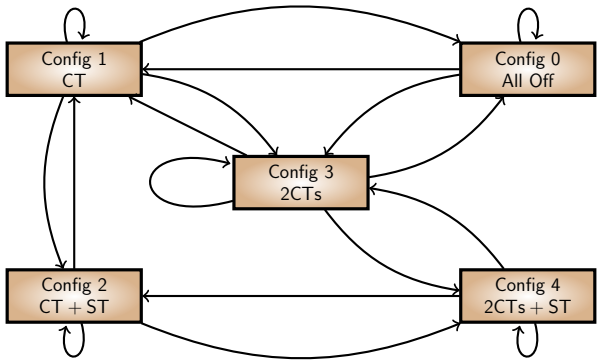

Figure 4: Configuration-based Model

The configuration-based model can clearly describe the transition process of a combined-cycle unit among different modes (i.e., configurations or states). California ISO and ERCOT[2] have implemented the configuration-based model in their markets (see, e.g., [25] and [14]). As compared to the aggregated model and pseudo unit model approaches, the configuration-based model significantly increases the computational time to solve the UC problem including both combined-cycle and traditional thermal units [8]. Recently, research progress has been made in providing tighter MILP formulations of configuration-based combined-cycle units (see [25] and [20]). However, the

[2]Electric Reliability Council of Texas, an ISO managing the electric power transmission network mainly in Texas, USA.

configuration-based model still faces challenges in terms of accuracy because this approach cannot capture the operating constraints and costs for each individual turbine, as indicated in [17]. More specifically, the configuration-based model is still an "aggregated" model that does not track the start-up/shut-down process of each individual turbine, and thus cannot capture the min-up/-down time requirement for each turbine, nor can it capture the time-dependent start-up cost for each CT. As a result, it may lead to infeasibility issue by providing the ISOs a practically infeasible solution. The market participants may also face such an infeasibility issue since when they submit bidding offers to the ISOs based on the min-up/-down time requirements of each turbine, it may turn out that these offers are infeasible for the configuration-based model that will be run by the ISOs. As the electricity market develops, more accurate and efficient combined-cycle unit models are required so that a lower operation cost can be achieved and more accurate offline simulations can be conducted. For instance, CAISO is recently working on a new project named *Commitment Cost Enhancements Phase 3* [6] and requires a combined-cycle unit model that can capture the accurate transition costs, which generally refer to the time-dependent start-up costs of CTs. Unfortunately, the configuration-based model is unable to achieve this.

In order to improve the computational performance and accuracy of the combined-cycle unit model, the fourth modeling approach, i.e., the edge-based model, is proposed in [12] to provide an accurate model for operating the combined-cycle units. This model first constructs the state transitions of the combined-cycle unit in a graph, then tracks the operating status of each individual turbine by using each arc in the transition graph to define a corresponding decision variable indicating the status of this arc, and finally builds the MILP formulation. These arcs can also represent the transition relationships among CTs and STs. As compared to the previous three models, this new modeling framework can exactly describe the operating physical constraints including the min-up/-down time requirements and time-dependent start-up costs of each CT and ST in the whole combined-cycle unit by tracking its start-up and shut-down processes. Nevertheless, the edge-based model is still challenged in the computational performance when the number of CTs and STs increases and the number of combined-cycle units increases in the unit commitment model. In fact, the number of combined-cycle units is increasing significantly in the U.S. ISOs' generation portfolio [6], which calls for more advanced approaches to improve the efficiency.

In this paper, therefore, we focus on improving the computational efficiency based on the most updated combined-cycle unit model (i.e., the edge-based formulation), which has the advantage of exactly tracking the operating physical constraints over other existing models. More specifi-

cally, we improve the computational performance by deriving better constraints for the edge-based formulation and strong valid inequalities as cutting planes to strengthen the formulation. Both of them take advantage of the physical characteristics of each individual turbine and the special structure of the state transition graph for the problem. Nowadays, commercial MILP solvers such as CPLEX have been used to solve UC problems by most ISOs in the U.S. [15]. The ISOs are continually seeking improved methods to better schedule the combined-cycle units, because a small improvement, even 1% in the cost of a final generation schedule, will result in huge savings in total due to the large total generation amount involved (e.g., result in $0.2 billion annually for MISO [8]). Thus, it is crucial to derive strong formulations that can solve the problem in a short time.

Most MILP solvers implement the branch-and-bound algorithm associated with the linear programming (LP) relaxation at each branching node, including the root node. A strong formulation is able to provide a better LP relaxation bound (e.g., a better lower bound for a minimization MILP problem), which further helps obtain a better solution in a short time during the branch-and-bound process. Research progress has been made on how to strengthen the traditional thermal unit commitment formulation (e.g., [26, 30, 32, 24]). For instance, in [5] and [21], a classic MILP formulation is developed with three binary variables (i.e., start-up, shut-down, and the unit on-line/offline status). In [27], the min-up/-down time polytope based on two binary variables is strengthened. In [7], a computationally efficient MILP formulation with a single binary variable for each unit status is proposed. Recently, in [15], a tight unit commitment formulation is studied by the polyhedral approximation of the perspective reformulation. In addition, several families of strong valid ramping-rate inequalities are derived to tighten the formulation in [22] and [9] and strong valid inequalities for the polytope including all of the min-up/-down time, ramping rate, and capacity constraints are derived in [23].

However, the study of deriving the strong valid inequalities for combined-cycle units is limited. In this paper, we strengthen the edge-based formulation for a combined-cycle unit to improve its computational performance, thereby helping the industry benefit from the exact combined-cycle unit model and large savings. We summarize our contributions as follows:

1. We derive tighter min-up/-down time and ramping rate constraints for the edge-based model of combined-cycle units.

2. We provide several families of strong valid inequalities in terms of ramping rates for the combined-cycle unit by exploring the special structure of the state transition graph of a combined-cycle unit. We show that the inequalities are valid for the original formulation and

facet-defining under mild conditions.

3. We conduct computational experiments on different data sets, which verify the effectiveness of our proposed formulation in solving large-scale unit commitment problems with combined-cycle units included.

Note here that since we focus on the edge-based combined-cycle unit model, which is different from other alternatives, the proposed strong formulation is also different from that for other approaches, such as [25] and [20] based on configuration-based model. The remaining part of this paper is organized as follows. In Section 2, we describe the original edge-based formulation. In Section 3, we describe our innovative tighter constraints and strong valid inequalities for combined-cycle units. In Section 4, we report and analyze our computational results. Finally, we conclude this study in Section 5.

2 The Edge-Based Formulation of a Combined-Cycle Unit

In this section, we first introduce the basic principle of the edge-based formulation for a combined-cycle unit as described in [12]. Then we characterize the relationships among the statuses of a combined-cycle unit. Finally we describe the mathematical formulation.

The edge-based formulation relies on the state transition graph of a combined-cycle unit with multiple CTs and STs, where a node represents a configuration (i.e., committing a subset of CTs and STs online) and an arc (denoted by $a(n, m)$) represents a possible transition from configurations n to m. For example, we use Fig. 5 to display all possible configurations and corresponding transitions for a combined-cycle unit with 2 CTs and 1 ST. The whole combined-cycle unit works on one of the configurations at each time period. In the edge-based formulation, each configuration is considered as a pseudo thermal unit, and a decision variable is designed for each transition arc in the graph to track the transition process within the whole combined-cycle unit.

To mathematically describe the edge-based formulation, in the state transition graph, we let $\mathcal{A}$ represent the set of all the arcs, $\mathcal{A}_k^{\text{all}}$ represent the set of arcs linked to configuration k, $\mathcal{A}_k^{\text{in}}$ represent the set of incoming arcs of configuration k, $\mathcal{A}_k^{\text{out}}$ represent the set of outgoing arcs of configuration k, $\mathcal{A}_k^{\text{sl}}$ represent the set of self-loop arcs of configuration k, $\mathcal{A}_i^{\text{sd}}$ represent the set of arcs indicating turbine i shuts down, $\mathcal{A}_i^{\text{su}}$ represent the set of arcs indicating turbine i starts up, $\mathcal{A}_i^{\text{on}}$ represent the set of arcs indicating turbine i keeps online, and $\mathcal{A}_i^{\text{off}}$ represent the set of arcs indicating turbine i keeps offline. Note here that neither $\mathcal{A}_k^{\text{in}}$ nor $\mathcal{A}_k^{\text{out}}$ includes the self-loop arcs, i.e., the arcs in $\mathcal{A}_k^{\text{sl}}$. In

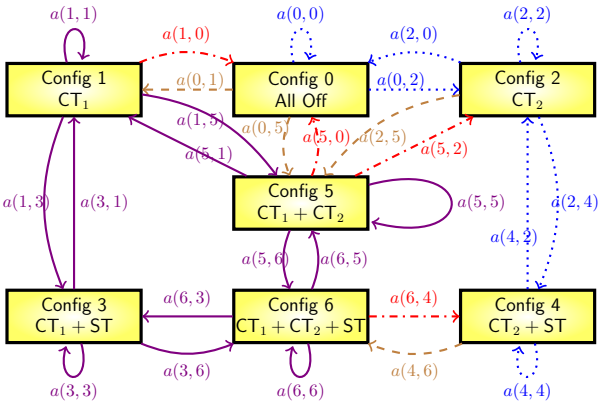

Figure 5: State Transition Graph

addition, we let $\mathcal{C}$ represent the set of all the configurations, $\mathcal{C}_i^{\text{off}}$ represent the set of configurations indicating that turbine i is offline, and $\mathcal{C}_i^{\text{on}}$ represent the set of configurations indicating that turbine i is online.

In addition, for the combined-cycle unit, we let $\mathcal{U}^{\text{CT}}$ represent the set of its CTs and $\mathcal{U}^{\text{ST}}$ represent the set of its STs. We also let $\mathcal{T}$ represent the set of scheduling time periods and $\mathcal{T}_{\text{end}}$ represent the last time period. For the parameter settings of the combined-cycle unit, we let $\underline{P}_k$ represent the minimal power output of configuration k, $\bar{P}_k$ represent the maximal power output of configuration k, and $\bar{P}^c$ represent its total capacity. For each turbine $i \in \mathcal{U}^{\text{CT}} \cup \mathcal{U}^{\text{ST}}$, we let T_{mu}^i represent its min-up time once it starts up, T_{md}^i represent its min-down time once it shuts down. The start-up cost of a turbine depends on how long this turbine has been offline right before the start-up and approximately it is a step function of the offline time length, with three steps (called "hot", "warm", and "cold"). Thus, for turbine i, we use $\bar{V}_1^i$ to represent its hot start-up cost (representing the start-up cost if the offline time length is short), $\delta_{1,2}^i$ to represent the difference between the warm and hot start-up costs, $\delta_{2,3}^i$ to represent the difference between the cold and warm start-up costs, $\underline{V}^i$ represent its shut-down cost, T_{c}^i represent its cold start time, and T_{w}^i represent its warm start time. In the state transition graph, we let RD^a represent the ramping down limit of arc a and RU^a represent the ramping up limit of arc a. Note that all the parameters are positive.

The decision variables of the edge-based formulation mainly include the status of each arc in the state transition graph. That is, we let binary variable z_t^a represent the online/offline status of arc a at time period t. In addition, for the continuous variables of a combined-cycle unit, we let Θ represent its operating cost. Also, for the combined-cycle unit, we let p_t represent its generation amount, p_t^k represent the generation amount of configuration k, ϕ_t^k represent the generation cost of

configuration k, and φ_t^i represent the start-up cost of turbine i at each time period t.

Furthermore, we characterize the relationships among different groups of transition arcs of the state transition graph, which will be used for later theoretical proofs in the remaining part of this paper. In the edge-based formulation, we use the decision variables corresponding to all the arcs to track the status of each turbine, which has four possible transition statuses in total, i.e., start-up, shut-down, keeping online, and keeping offline. Accordingly, all these arcs can be divided into four corresponding groups. For instance, we use CT_1 as an example to explain these four groups as shown in Fig. 5. The dash dotted arcs represent the shut-down process of turbine CT_1. The dash arcs represent the start-up process of turbine CT_1. The solid arcs represent CT_1 keeps online. The dotted arcs represent CT_1 keeps offline. Finally, we can summarize the relationships among these four groups as indicated in the following (1) - (4) and these relationships can be easily verified based on the state transition graph. Meanwhile, we summarize all the notations described above in Appendix B for reference.

$$\emptyset = \mathcal{A}_i^{\kappa} \cap \mathcal{A}_i^{\tau},\ \forall \kappa, \tau \in \{\mathrm{su}, \mathrm{sd}, \mathrm{on}, \mathrm{off}\}, \kappa \neq \tau, \forall i \in \mathcal{U}^{\mathrm{CT}} \cup \mathcal{U}^{\mathrm{ST}}. \tag{1}$$

$$\mathcal{A} = \mathcal{A}_i^{\mathrm{su}} \cup \mathcal{A}_i^{\mathrm{sd}} \cup \mathcal{A}_i^{\mathrm{on}} \cup \mathcal{A}_i^{\mathrm{off}},\ \forall i \in \mathcal{U}^{\mathrm{CT}} \cup \mathcal{U}^{\mathrm{ST}}. \tag{2}$$

$$\bigcup_{k \in \mathcal{C}_i^{\mathrm{off}}} \mathcal{A}_k^{\mathrm{all}} = \mathcal{A}_i^{\mathrm{su}} \cup \mathcal{A}_i^{\mathrm{sd}} \cup \mathcal{A}_i^{\mathrm{off}},\ \forall i \in \mathcal{U}^{\mathrm{CT}} \cup \mathcal{U}^{\mathrm{ST}}. \tag{3}$$

$$\bigcup_{k \in \mathcal{C}_i^{\mathrm{on}}} \mathcal{A}_k^{\mathrm{all}} = \mathcal{A}_i^{\mathrm{su}} \cup \mathcal{A}_i^{\mathrm{sd}} \cup \mathcal{A}_i^{\mathrm{on}},\ \forall i \in \mathcal{U}^{\mathrm{CT}} \cup \mathcal{U}^{\mathrm{ST}}. \tag{4}$$

Accordingly, the edge-based formulation for a combined-cycle unit can be summarized as follows:

$$\sum_{a \in \mathcal{A}} z_t^a = 1,\ \forall t, \tag{5}$$

$$\sum_{a \in (\mathcal{A}_k^{\mathrm{in}} \bigcup \mathcal{A}_k^{\mathrm{sl}})} z_t^a = \sum_{a \in (\mathcal{A}_k^{\mathrm{out}} \bigcup \mathcal{A}_k^{\mathrm{sl}})} z_{t+1}^a,\ \forall k \in \mathcal{C}, \forall t, \tag{6}$$

$$\sum_{a \in \bigcup_{k \in \mathcal{C}_i^{\mathrm{off}}} \mathcal{A}_k^{\mathrm{all}}} z_\tau^a \leq 1 - \sum_{a \in \mathcal{A}_i^{\mathrm{su}}} z_t^a,\ \forall i \in \mathcal{U}^{\mathrm{CT}} \cup \mathcal{U}^{\mathrm{ST}},\ \forall \tau \in \{t+1, \cdots, \min\{\mathcal{T}_{\mathrm{end}}, T_{\mathrm{mu}}^i + t - 1\}\},\ \forall t, \tag{7}$$

$$\sum_{a \in \bigcup_{k \in \mathcal{C}_i^{\mathrm{on}}} \mathcal{A}_k^{\mathrm{all}}} z_\tau^a \leq 1 - \sum_{a \in \mathcal{A}_i^{\mathrm{sd}}} z_t^a,\ \forall i \in \mathcal{U}^{\mathrm{CT}} \cup \mathcal{U}^{\mathrm{ST}},\ \forall \tau \in \{t+1, \cdots, \min\{\mathcal{T}_{\mathrm{end}}, T_{\mathrm{md}}^i + t - 1\}\},\ \forall t, \tag{8}$$

$$p_t = \sum_{k \in \mathcal{C}} p_t^k,\ \forall t, \tag{9}$$

$$\underline{P}_k \left(\sum_{a \in (\mathcal{A}_k^{\mathrm{in}} \bigcup \mathcal{A}_k^{\mathrm{sl}})} z_t^a \right) \leq p_t^k \leq \bar{P}_k \left(\sum_{a \in (\mathcal{A}_k^{\mathrm{in}} \bigcup \mathcal{A}_k^{\mathrm{sl}})} z_t^a \right),\ \forall k \in \mathcal{C}, \forall t, \tag{10}$$

$$p_{t+1} - p_t \leq \mathrm{RU}^a z_{t+1}^a + \bar{P}^c (1 - z_{t+1}^a),\ \forall a \in \mathcal{A}, \forall t, \tag{11}$$

$$p_t - p_{t+1} \le \mathrm{RD}^a z^a_{t+1} + \bar{P}^c(1 - z^a_{t+1}),\ \forall a \in \mathcal{A}, \forall t, \tag{12}$$

$$\Theta = \sum_{t\in\mathcal{T}} \left(\sum_{k\in\mathcal{C}} \phi^k_t(p^k_t) + \sum_{i\in\mathcal{U}^{\mathrm{CT}}} \left(\varphi^i_t + \underline{V}^i \sum_{a\in\mathcal{A}^{\mathrm{sd}}_i} z^a_t \right) \right), \tag{13}$$

$$\varphi^i_t \ge \bar{V}^i_1 \sum_{a\in\mathcal{A}^{\mathrm{su}}_i} z^a_t,\ \forall i \in \mathcal{U}^{\mathrm{CT}},\ \forall t, \tag{14}$$

$$\varphi^i_t \ge (\bar{V}^i_1 + \delta^i_{1,2}) \left(\sum_{a\in\mathcal{A}^{\mathrm{su}}_i} z^a_t - \sum_{\tau=T^i_{\mathrm{md}}+1}^{T^i_{\mathrm{w}}} \sum_{a\in\mathcal{A}^{\mathrm{sd}}_i} z^a_{t-\tau} \right),\ \forall i \in \mathcal{U}^{\mathrm{CT}},\ \forall t, \tag{15}$$

$$\varphi^i_t \ge (\bar{V}^i_1 + \delta^i_{1,2} + \delta^i_{2,3}) \left(\sum_{a\in\mathcal{A}^{\mathrm{su}}_i} z^a_t - \sum_{\tau=T^i_{\mathrm{md}}+1}^{T^i_{\mathrm{c}}} \sum_{a\in\mathcal{A}^{\mathrm{sd}}_i} z^a_{t-\tau} \right),\ \forall i \in \mathcal{U}^{\mathrm{CT}}, \forall t. \tag{16}$$

In the above formulation, constraints (5) indicate that only one of the arcs in $\mathcal{A}$ can be active at each time period since the combined-cycle unit moves along exactly one arc at each time period. Constraints (6) keep tracking the transition process corresponding to each time period t and configuration k, indicating that if a mode is online at the current period, then in the next time period it can either stay in the current mode or move to another mode. Constraints (7) and (8) enforce the min-up/-down time requirements for each turbine, respectively. Since each configuration is a pseudo thermal unit, the generation capacity restrictions of these pseudo thermal units are represented in constraints (9) - (10). Equations (9) provide the representation of the generation amount of the whole combined-cycle unit. Constraints (10) restrict the generation amount of each configuration from below and above respectively. Constraints (11) and (12) describe ramping up/down rate restrictions, respectively. Constraint (13) explicitly describes the total operating cost that includes generation cost (i.e., $\sum_{t\in\mathcal{T}}\sum_{k\in\mathcal{C}} \phi^k_t(p^k_t)$), start-up cost (i.e., $\sum_{t\in\mathcal{T}}\sum_{i\in\mathcal{U}^{\mathrm{CT}}} \varphi^i_t$), and shut-down cost (i.e., $\sum_{t\in\mathcal{T}}\sum_{i\in\mathcal{U}^{\mathrm{CT}}} \left(\underline{V}^i \sum_{a\in\mathcal{A}^{\mathrm{sd}}_i} z^a_t\right)$). More specifically, $\phi^k_t(p^k_t)$ is a nondecreasing quadratic function of p^k_t, which can be approximated by a piecewise linear function. The detailed time-dependent start-up costs are described in constraints (14) - (16). In particular, considering turbine i starting up at time t, the start-up cost will be (1) $\bar{V}^i_1$ (i.e., hot start-up cost) if turbine i has been offline between $t - T^i_{\mathrm{w}}$ and $t - T^i_{\mathrm{md}} - 1$; (2) $\bar{V}^i_1 + \delta^i_{1,2}$ (i.e., warm start-up cost) if turbine i has been offline between $t - T^i_{\mathrm{c}}$ and $t - T^i_{\mathrm{w}} - 1$; (3) $\bar{V}^i_1 + \delta^i_{1,2} + \delta^i_{2,3}$ (i.e., cold start-up cost) otherwise. Finally, we define the integer feasible region with constraints (5) - (16) as $\mathcal{Q}$ and the convex hull of $\mathcal{Q}$ is denoted by $\mathrm{conv}(\mathcal{Q})$.

Remark 1. *In formulation* (5) - (16)*, we present all the constraints to capture the physical characteristics of a combined-cycle unit, rather than solving an optimization problem. Based on* (5) - (16)*, we provide our strengthened formulation in Section 3. Thus, network constraints (e.g.,*

demand balance and transmission line constraints) appearing in a network-constrained UC model are not provided here. Instead a complete UC model considering both traditional thermal units and combined-cycle units is provided in Appendix B.1, where the objective is to minimize the total operating cost (including Θ for each combined-cycle unit) while satisfying all the physical and network constraints. The computational experiments to solve the complete UC model will be performed in Section 4.

Remark 2. *The edge-based formulation above, i.e.,* (5) - (16)*, provides a different modeling framework from other formulations for the operations of combined-cycle units, e.g., the configuration-based formulation. It follows that our proposed tighter constraints and strong valid inequalities in Section 3 are new and different from the existing studies since our results are specified for the edge-based formulation.*

3 Strengthened Formulation

In this section, we derive tighter constraints for the edge-based formulation and several families of strong valid inequalities to strengthen the formulation, which eventually improve the computational efficiency significantly to solve the UC problem with combined-cycle units embedded.

3.1 Tighter Constraints

In this subsection, we propose three sets of constraints to replace the corresponding original ones, namely the min-up time, min-down time, and ramping rate constraints, i.e., (7) - (8) and (11) - (12). We show that our proposed constraints are tighter than the original ones by providing theoretical proofs.

3.1.1 Min-up Time Constraints

We propose a set of tighter min-up time constraints in the following proposition.

Proposition 1. *The inequalities*

$$\sum_{\kappa=1}^{T^i_{mu}-1} \sum_{a\in\mathcal{A}^{su}_i} z^a_{t-\kappa} \leq 1 - \sum_{a\in\bigcup_{k\in\mathcal{C}^{off}_i}\mathcal{A}^{all}_k} z^a_t, \ \forall i \in \mathcal{U}^{CT}\cup\mathcal{U}^{ST}, \forall t \in \{T^i_{mu},\cdots,\mathcal{T}_{end}\}, \tag{17}$$

are tighter than constraints (7).

Motivated by the logic developed by [27] for the traditional thermal units, we develop tighter min-up time constraints for each turbine in a combined-cycle unit as shown in (17). The basic logic of (17) can be described as: if turbine i is online at time period t, then this turbine starts up at most once during time interval $[t-T^i_{\rm mu}+1, t-1]$. Thus, in the transition graph, if one of the arcs in $\mathcal{A}^{\rm su}_i$, representing the start-up process of turbine i, is active during time interval $[t-T^i_{\rm mu}+1, t-1]$, then arcs connected to the configurations without turbine i (i.e., $\bigcup_{k\in\mathcal{C}^{\rm off}_i}\mathcal{A}^{\rm all}_k$) cannot be active at t. In the following part, we show that constraints (17) are tighter than constraints (7).

Proof. To begin with, we rewrite constraints (7) as follows:

$$\sum_{a\in\mathcal{A}^{\rm su}_i} z^a_s \le 1 - \sum_{a\in\bigcup_{k\in\mathcal{C}^{\rm off}_i}\mathcal{A}^{\rm all}_k} z^a_\tau,\ \forall i\in\mathcal{U}^{\rm CT}\cup\mathcal{U}^{\rm ST}, \tag{18}$$
$$\forall\tau\in\{s+1,\cdots,\min\{\mathcal{T}_{\rm end}, T^i_{\rm mu}+s-1\}\}, \forall s\in\mathcal{T}.$$

By introducing $\kappa\in\{1,\cdots,T^i_{\rm mu}-1\}$, we reformulate constraints (18) as (19).

$$\sum_{a\in\mathcal{A}^{\rm su}_i} z^a_s \le 1 - \sum_{a\in\bigcup_{k\in\mathcal{C}^{\rm off}_i}\mathcal{A}^{\rm all}_k} z^a_{s+\kappa},\ \forall i\in\mathcal{U}^{\rm CT}\cup\mathcal{U}^{\rm ST}, \tag{19}$$
$$\forall\kappa\in\{1,\cdots,T^i_{\rm mu}-1\}, s+\kappa\le\mathcal{T}_{\rm end}, \forall s\in\mathcal{T}.$$

Then, we replace $s+\kappa$ with t to obtain (20).

$$\sum_{a\in\mathcal{A}^{\rm su}_i} z^a_{t-\kappa} \le 1 - \sum_{a\in\bigcup_{k\in\mathcal{C}^{\rm off}_i}\mathcal{A}^{\rm all}_k} z^a_t,\ \forall i\in\mathcal{U}^{\rm CT}\cup\mathcal{U}^{\rm ST}, \tag{20}$$
$$\forall\kappa\in\{1,\cdots,T^i_{\rm mu}-1\}, t-\kappa\ge 1, \forall t\in\{2,\cdots,\mathcal{T}_{\rm end}\}.$$

Therefore, we only need to show inequalities (17) are tighter than inequalities (20). We finish it by considering the following two cases.

First, we consider $t\in\{T^i_{\rm mu},\cdots,\mathcal{T}_{\rm end}\}$. Then we can remove the condition $t-\kappa\ge 1$ and obtain (21) from (20) as follows.

$$\sum_{a\in\mathcal{A}^{\rm su}_i} z^a_{t-\kappa} \le 1 - \sum_{a\in\bigcup_{k\in\mathcal{C}^{\rm off}_i}\mathcal{A}^{\rm all}_k} z^a_t,\ \forall i\in\mathcal{U}^{\rm CT}\cup\mathcal{U}^{\rm ST}, \tag{21}$$
$$\forall\kappa\in\{1,\cdots,T^i_{\rm mu}-1\}, \forall t\in\{T^i_{\rm mu},\cdots,\mathcal{T}_{\rm end}\}.$$

It is easy to observe that constraints (21) are dominated by constraints (17).

Next, we consider $t\in\{2,\cdots,T^i_{\rm mu}-1\}$. Note here that (20) can be rewritten as follows.

$$\sum_{a\in\mathcal{A}^{\rm su}_i} z^a_{t-\kappa} \le 1 - \sum_{a\in\bigcup_{k\in\mathcal{C}^{\rm off}_i}\mathcal{A}^{\rm all}_k} z^a_t,\ \forall i\in\mathcal{U}^{\rm CT}\cup\mathcal{U}^{\rm ST}, \tag{22}$$

$$\forall \kappa \in \{1, \cdots, t-1\}, \forall t \in \{2, \cdots, T^i_{\mathrm{mu}} - 1\}.$$

In constraints (22), we have $\kappa \in \{1, \cdots, t-1\}$ due to $t - 1 < T^i_{\mathrm{mu}} - 1$ and $\kappa \leq t - 1$. Then, it is easy to check that constraints (22) are dominated by (23), which are equivalent to (24).

$$\sum_{\kappa=1}^{t-1} \sum_{a \in \mathcal{A}_i^{\mathrm{su}}} z^a_{t-\kappa} \leq 1 - \sum_{a \in \bigcup_{k \in \mathcal{C}_i^{\mathrm{off}}} \mathcal{A}_k^{\mathrm{all}}} z^a_t, \ \forall i \in \mathcal{U}^{\mathrm{CT}} \cup \mathcal{U}^{\mathrm{ST}}, \forall t \in \{2, \cdots, T^i_{\mathrm{mu}} - 1\}. \tag{23}$$

$$\sum_{\omega=1}^{t-1} \sum_{a \in \mathcal{A}_i^{\mathrm{su}}} z^a_{\omega} \leq 1 - \sum_{a \in \bigcup_{k \in \mathcal{C}_i^{\mathrm{off}}} \mathcal{A}_k^{\mathrm{all}}} z^a_t, \ \forall i \in \mathcal{U}^{\mathrm{CT}} \cup \mathcal{U}^{\mathrm{ST}}, \forall t \in \{2, \cdots, T^i_{\mathrm{mu}} - 1\}. \tag{24}$$

Now we show an equivalent formulation of constraints (24) is dominated by (17). To that end, we first rewrite the left hand side (LHS) of constraints (24) by using the following logic relationship as shown in constraints (25), which are further equivalent to (26) by taking summation over $\omega \in [2, t]$.

$$\sum_{a \in \mathcal{A}_i^{\mathrm{su}} \cup \mathcal{A}_i^{\mathrm{on}}} z^a_{t+1} - \sum_{e \in \mathcal{A}_i^{\mathrm{su}} \cup \mathcal{A}_i^{\mathrm{on}}} z^a_t + \sum_{a \in \mathcal{A}_i^{\mathrm{sd}}} z^a_{t+1} = \sum_{a \in \mathcal{A}_i^{\mathrm{su}}} z^a_{t+1}, \ \forall t \in \mathcal{T}, \forall i \in \mathcal{U}^{\mathrm{CT}} \cup \mathcal{U}^{\mathrm{ST}}. \tag{25}$$

$$\sum_{\omega=2}^{t} \sum_{a \in \mathcal{A}_i^{\mathrm{su}}} z^a_{\omega} = \sum_{a \in \mathcal{A}_i^{\mathrm{su}} \cup \mathcal{A}_i^{\mathrm{on}}} z^a_t - \sum_{a \in \mathcal{A}_i^{\mathrm{su}} \cup \mathcal{A}_i^{\mathrm{on}}} z^a_1 + \sum_{\omega=2}^{t} \sum_{a \in \mathcal{A}_i^{\mathrm{sd}}} z^a_{\omega}, \ \forall t \in \mathcal{T}, \forall i \in \mathcal{U}^{\mathrm{CT}} \cup \mathcal{U}^{\mathrm{ST}}. \tag{26}$$

$$\sum_{\omega=1}^{t} \sum_{a \in \mathcal{A}_i^{\mathrm{su}}} z^a_{\omega} = \sum_{e \in \mathcal{A}_i^{\mathrm{su}} \cup \mathcal{A}_i^{\mathrm{on}}} z^a_t - \sum_{a \in \mathcal{A}_i^{\mathrm{on}}} z^a_1 + \sum_{\omega=2}^{t} \sum_{a \in \mathcal{A}_i^{\mathrm{sd}}} z^a_{\omega}, \ \forall t \in \mathcal{T}, \forall i \in \mathcal{U}^{\mathrm{CT}} \cup \mathcal{U}^{\mathrm{ST}}. \tag{27}$$

By moving the item $\sum_{a \in \mathcal{A}_i^{\mathrm{su}}} z^a_1$ to the LHS of constraints (26), we obtain (27). Therefore, we can reformulate constraints (24) as constraints (28) at given time period t by moving the item $\sum_{a \in \mathcal{A}_i^{\mathrm{su}}} z^a_t$ in (24) to the LHS based on the relationships indicated by constraints (3). Furthermore, we can rewrite constraints (28) as (29) by using constraints (27).

$$\sum_{\omega=1}^{t} \sum_{a \in \mathcal{A}_i^{\mathrm{su}}} z^a_{\omega} \leq 1 - \sum_{a \in \mathcal{A}_i^{\mathrm{sd}} \cup \mathcal{A}_i^{\mathrm{off}}} z^a_t, \ \forall t \in \{2, \cdots, T^i_{\mathrm{mu}} - 1\}, \forall i \in \mathcal{U}^{\mathrm{CT}} \cup \mathcal{U}^{\mathrm{ST}}, \tag{28}$$

$$\sum_{a \in \mathcal{A}_i^{\mathrm{su}} \cup \mathcal{A}_i^{\mathrm{on}}} z^a_t - \sum_{a \in \mathcal{A}_i^{\mathrm{su}} \cup \mathcal{A}_i^{\mathrm{on}}} z^a_1 + \sum_{\omega=2}^{t} \sum_{a \in \mathcal{A}_i^{\mathrm{sd}}} z^a_{\omega} \leq 1 - \sum_{a \in \mathcal{A}_i^{\mathrm{sd}} \cup \mathcal{A}_i^{\mathrm{off}}} z^a_t, \ \forall t \in \{2, \cdots, T^i_{\mathrm{mu}} - 1\}, \forall i \in \mathcal{U}^{\mathrm{CT}} \cup \mathcal{U}^{\mathrm{ST}}. \tag{29}$$

Based on (5) and (2), we can observe that constraints (29) are equivalent to constraints (30).

$$\sum_{\omega=2}^{t} \sum_{a \in \mathcal{A}_i^{\mathrm{sd}}} z^a_{\omega} \leq \sum_{e \in \mathcal{A}_i^{\mathrm{su}} \cup \mathcal{A}_i^{\mathrm{on}}} z^a_1, \ \forall t \in \{2, \cdots, T^i_{\mathrm{mu}} - 1\}, \forall i \in \mathcal{U}^{\mathrm{CT}} \cup \mathcal{U}^{\mathrm{ST}}. \tag{30}$$

By following the similar process to obtain constraints (30), we get an equivalent formulation (31) of constraints (17) when $t = T^i_{\mathrm{mu}}$. Obviously, the constraints in (30) at given time periods

$t \in \{2, \cdots, T^i_{\text{mu}} - 1\}$ are dominated by constraints (31).

$$\sum_{\omega=2}^{T^i_{\text{mu}}} \sum_{a \in \mathcal{A}^{\text{sd}}_i} z^a_\omega \leq \sum_{e \in \mathcal{A}^{\text{su}}_i \cup \mathcal{A}^{\text{on}}_i} z^a_1, \ \forall i \in \mathcal{U}^{\text{CT}} \cup \mathcal{U}^{\text{ST}}. \tag{31}$$

The proof is done. □

3.1.2 Min-down Time Constraints

By following the similar idea as the reformulation of min-up time constraints, we derive tighter constraints for min-down time requirements in (32).

Proposition 2. *The inequalities*

$$\sum_{\kappa=1}^{T^i_{md}-1} \sum_{a \in \mathcal{A}^{sd}_i} z^a_{t-\kappa} \leq 1 - \sum_{a \in \bigcup_{k \in \mathcal{C}^{on}_i} \mathcal{A}^{all}_k} z^a_t, \ \forall i \in \mathcal{U}^{CT} \cup \mathcal{U}^{ST}, \forall t \in \{T^i_{md}, \cdots, \mathcal{T}_{end}\}, \tag{32}$$

are tighter than constraints (8).

Constraints (32) indicate that if one of the arcs in $\mathcal{A}^i_{\text{sd}}$, representing the shut-down process of turbine i, is active during time interval $[t - T^i_{\text{md}} + 1, t - 1]$, then arcs connected to the configurations with turbine i (i.e., $\bigcup_{k \in \mathcal{C}^{\text{on}}_i} \mathcal{A}^{\text{all}}_k$) cannot be active. This means the configurations with turbine i must be offline at time period t, when turbine i shuts down at time interval $[t - T^i_{\text{md}} + 1, t - 1]$. Due to the similar logic with the tighter min-up constraints (17), we can show that constraints (32) are tighter than constraints (8) by similarly following the proof for Proposition 1 in two steps: 1) rewrite (8) into

$$\sum_{a \in \mathcal{A}^{\text{sd}}_i} z^a_{t-\kappa} \leq 1 - \sum_{a \in \bigcup_{k \in \mathcal{C}^{\text{on}}_i} \mathcal{A}^{\text{all}}_k} z^a_t, \ \forall i \in \mathcal{U}^{\text{CT}} \cup \mathcal{U}^{\text{ST}}, \tag{33}$$
$$\forall \kappa \in \{1, \cdots, T^i_{\text{md}} - 1\}, t - \kappa \geq 1, \forall t \in \{2, \cdots, \mathcal{T}_{\text{end}}\};$$

and 2) show constraints (32) are tighter than (33). Thus we omit the detailed proof here.

3.1.3 Ramping Rate Constraints

As mentioned previously, the edge-based formulation tracks the transition process of a combined-cycle unit by recording the status of each arc. The status of each arc indicates the operating status of the combined-cycle unit, which further determines which ramping rate limit (corresponding to each arc) affects the change of the generation amount at each time period. Hence, ramping rate constraints (11) and (12) use the arc decision variables to make the choice of ramping rate limits.

Instead of using big-M method (i.e., $\bar{P}^c$) as shown in (11) and (12), we propose two other tighter ramping rate constraints.

Proposition 3. *The inequalities*

$$p_{t+1} - p_t \leq \sum_{a \in \mathcal{A}} RU^a z^a_{t+1}, \ \forall t \in \mathcal{T}, \tag{34}$$

$$p_t - p_{t+1} \leq \sum_{a \in \mathcal{A}} RD^a z^a_{t+1}, \ \forall t \in \mathcal{T}, \tag{35}$$

represent tighter ramping up/down rate constraints than (11) *and* (12)*, respectively.*

Because only one of the arcs in the transition graph can be active at each time period t as shown in (5), only one item in the right-hand side of (34) can be positive and all others would be zero. This positive item represents the active arc that provides the ramping up rate limit. The same analysis can be applied to ramping down constraints (35).

Proof. By considering constraints (5) and the fact that $\bar{P}^c \geq \max\{\mathrm{RU}^a, \mathrm{RD}^a\}, \forall a$, it is easy to check that constraints (34) and (35) dominate constraints (11) and (12), respectively. □

Next, we further show the strength of our proposed tighter ramping rate constraints (34) and (35) by proving that they are facet-defining under certain conditions.

Proposition 4. *Inequalities* (34) *and* (35) *are facet-defining for the projection of polytope conv(*$\mathcal{Q}$*) onto set* $\mathcal{S} = \{z^a_{t+1}, p_{t+1}, p_t \ \forall a \in \mathcal{A}\}$ *when* $\underline{P}_n \leq \underline{P}_m + RU^{a(m,n)} \leq \bar{P}_n$ *for all* $a(m,n) \in \mathcal{A}$*, where* $\mathcal{S}$ *consists of all the variables describing inequalities* (34) *and* (35)*.*

Proof. As there are $|\mathcal{A}|+2$ variables and $\sum_{a \in \mathcal{A}} z^a_{t+1} = 1$, the dimension of $\mathcal{S}$ is $|\mathcal{A}|+1$. In order to prove that each inequality (34) is facet-defining for $\mathcal{S}$, we need $|\mathcal{A}|+1$ affinely independent points which satisfy $p_{t+1} - p_t = \sum_{a \in \mathcal{A}} \mathrm{RU}^a z^a_{t+1}$ at time period $t+1$ as shown in Table 1. Similarly, we can show that inequality (35) is facet-defining for the space S under mild conditions and thus we omit the corresponding details here. □

3.2 Strong Valid Inequalities

In this section, we derive several families of strong valid inequalities to further strengthen the edge-based formulation in multiple settings.

Table 1: $|\mathcal{A}|+1$ Affinely Independent Points

Points	z^a_{t+1}					p_{t+1}	p_t
	$a(m_1,n_1)$	$a(m_2,n_2)$	$\ddots$	$a(m_{\lvert\mathcal{A}\rvert-1},n_{\lvert\mathcal{A}\rvert-1})$	$a(m_{\lvert\mathcal{A}\rvert},n_{\mathcal{A}\rvert})$		
1	1	0	0	0	0	$\underline{P}_{m_1}+\mathrm{RU}^{a(m_1,n_1)}$	$\underline{P}_{m_1}$
2	0	1	0	0	0	$\underline{P}_{m_2}+\mathrm{RU}^{a(m_2,n_2)}$	$\underline{P}_{m_2}$
$\ddots$	0	0	$\ddots$	0	0	$\ddots$	$\ddots$
$\lvert\mathcal{A}\rvert-1$	0	0	0	1	0	$\underline{P}_{m_{\lvert\mathcal{A}\rvert-1}}+$ $\mathrm{RU}^{a(m_{\lvert\mathcal{A}\rvert-1},n_{\lvert\mathcal{A}\rvert-1})}$	$\underline{P}_{m_{\lvert\mathcal{A}\rvert-1}}$
$\lvert\mathcal{A}\rvert$	0	0	0	0	1	$\underline{P}_{m_{\lvert\mathcal{A}\rvert}}+$ $\mathrm{RU}^{a(m_{\lvert\mathcal{A}\rvert},n_{\lvert\mathcal{A}\rvert})}$	$\underline{P}_{m_{\lvert\mathcal{A}\rvert}}$
$\lvert\mathcal{A}\rvert+1$	1	0	0	0	0	$\underline{P}_{m_1}+$ $\mathrm{RU}^{a(m_1,n_1)}+\epsilon$	$\underline{P}_{m_1}+\epsilon$

3.2.1 Single-Arc Ramping Rate Inequalities

In Subsection 3.1.3, inequalities (34) and (35) focus on the change of generation amount p_t for the whole combined-cycle unit. Note that equations (9) indicate that only the online configuration of the combined-cycle unit provides the generation amount. Now, we focus on the change of generation amount p^k_t at each configuration of the combined-cycle unit. Given a specific arc $a(n,m)$, the whole combined-cycle unit transits from Configurations n to m. Accordingly, we focus on ramping rates and propose strong valid inequalities corresponding to this arc $a(n,m)$, named single-arc ramping rate inequalities.

Proposition 5. *The inequalities*

$$p^m_{t+1}-p^n_t \le RU^{a(n,m)} z^{a(n,m)}_{t+1} + \bar{P}_m\left(\sum_{a\in(\mathcal{A}^{in}_m \bigcup \mathcal{A}^{sl}_m)} z^a_{t+1}\right) - \underline{P}_n\left(\sum_{a\in(\mathcal{A}^{in}_n \bigcup \mathcal{A}^{sl}_n)} z^a_t\right) + \left(\underline{P}_n-\bar{P}_m\right) z^{a(n,m)}_{t+1}, \quad \forall a(n,m)\in\mathcal{A}, \forall t\in\mathcal{T}, \tag{36}$$

$$p^n_t-p^m_{t+1} \le RD^{a(n,m)} z^{a(n,m)}_{t+1} + \bar{P}_n\left(\sum_{a\in(\mathcal{A}^{in}_n \bigcup \mathcal{A}^{sl}_n)} z^a_t\right) - \underline{P}_m\left(\sum_{a\in(\mathcal{A}^{in}_m \bigcup \mathcal{A}^{sl}_m)} z^a_{t+1}\right) + \left(\underline{P}_m-\bar{P}_n\right) z^{a(n,m)}_{t+1}, \quad \forall a(n,m)\in\mathcal{A}, \forall t\in\mathcal{T}, \tag{37}$$

are valid for conv($\mathcal{Q}$). Furthermore, inequality (36) (resp. (37)) is facet-defining for the projection of polytope conv($\mathcal{Q}$) onto $\mathcal{S}=\{z^a_t, z^a_{t+1}, p^n_t, p^n_{t+1},\ \forall a\in\mathcal{A}\}$ when $\underline{P}_m \le \underline{P}_n + RU^{a(n,m)} < \bar{P}_m$ and $\bar{P}_m-\bar{P}_n < RU^{a(n,m)}$ (resp. $\underline{P}_n \le \underline{P}_m + RD^{a(n,m)} < \bar{P}_n$ and $\bar{P}_n-\bar{P}_m < RD^{a(n,m)}$), $\forall a(n,m)\in\mathcal{A}$, where $\mathcal{S}$ consists of all the variables describing (36) (resp. (37)).

Note here that it is not necessary to distinguish Configuration n from Configuration m in both inequalities (36) and (37). When $n = m$, it means the combined-cycle unit keeps working on one configuration between two consecutive time periods, where the ramping rate is from the corresponding configuration. When $n \neq m$, it means the combined-cycle unit transits from one configuration to another. In this case, the ramping rate is between these two configurations.

Proof. First, we show the validity of ramping up inequalities (36) for a given arc $a(n, m)$ by discussing four possible cases as follows.

Case 1: the combined-cycle unit works on Configuration n at time period t and works on Configuration m at $t+1$. It follows that arc $a(n, m)$ is active at $t+1$ in this case, and the ramping rate limit corresponding to arc $a(n, m)$ is selected to limit the generation amount change of the combined-cycle unit from t to $t+1$. Accordingly, we have $z_{t+1}^{a(n,m)} = 1$, $\sum_{a \in (\mathcal{A}_n^{\text{in}} \bigcup \mathcal{A}_n^{\text{sl}})} z_t^a = 1$, and $\sum_{a \in (\mathcal{A}_m^{\text{in}} \bigcup \mathcal{A}_m^{\text{sl}})} z_{t+1}^a = 1$. Then inequalities (36) convert to $p_{t+1}^m - p_t^n \leq \text{RU}^{a(n,m)}$, which is valid due to constraints (11).

Case 2: the combined-cycle unit works on Configuration n at time period t and does not work on Configuration m at $t+1$. It follows that arc $a(n, m)$ is not active at time period $t+1$ in this case, and the ramping rate limit corresponding to arc $a(n, m)$ will not be selected to limit the change of generation amount of the combined-cycle unit. Accordingly, we have $z_{t+1}^{a(n,m)} = 0$, $\sum_{a \in (\mathcal{A}_n^{\text{in}} \bigcup \mathcal{A}_n^{\text{sl}})} z_t^a = 1$, and $\sum_{a \in (\mathcal{A}_m^{\text{in}} \bigcup \mathcal{A}_m^{\text{sl}})} z_{t+1}^a = 0$. Then inequalities (36) convert to $-p_t^n \leq -\underline{P}_n$ which is valid due to constraints (10).

Case 3: the combined-cycle unit does not work on Configuration n at time period t. However, it works on Configuration m at time period $t+1$. Similar to Case 2, we have $z_{t+1}^{a(n,m)} = 0$, $\sum_{a \in (\mathcal{A}_n^{\text{in}} \bigcup \mathcal{A}_n^{\text{sl}})} z_t^a = 0$, and $\sum_{a \in (\mathcal{A}_m^{\text{in}} \bigcup \mathcal{A}_m^{\text{sl}})} z_{t+1}^a = 1$ in this case. Then inequalities (36) become $p_{t+1}^m \leq \bar{P}_m$, which is valid due to constraints (10).

Case 4: the combined-cycle unit neither works on Configuration n at time period t nor works on Configuration m at time period $t+1$. It follows that we have $z_{t+1}^{a(n,m)} = 0$, $\sum_{a \in (\mathcal{A}_n^{\text{in}} \bigcup \mathcal{A}_n^{\text{sl}})} z_t^a = 0$, and $\sum_{a \in (\mathcal{A}_m^{\text{in}} \bigcup \mathcal{A}_m^{\text{sl}})} z_{t+1}^a = 0$. Inequalities (36) become $0 \leq 0$, which is trivial.

These four cases cover all possible scenarios of inequalities (36) for a given arc $a(n, m)$. Similar analyses can be applied to inequalities (37) and thus are omitted here.

Next, we show inequalities (36) and (37) are facet-defining in Appendix A.1. □

3.2.2 Multi-Configuration Ramping Rate Inequalities

In Subsection 3.2.1, inequalities (36) and (37) study the ramping rate limits for a given arc. In this subsection, we extend the study to develop the ramping rate inequalities by considering a given configuration and its relationships with other configurations, named multi-configuration ramping rate inequalities.

Suppose that the whole combined-cycle unit works on Configuration m at time period $t+1$. As shown in Fig. 6, we know one of the incoming arcs, i.e., $a(n_1, m), a(n_2, m)$, and $a(n_3, m)$, or the self-loop arc $a(m, m)$ must be active at time period $t+1$. On the other hand, suppose that the combined-cycle unit works on Configuration n at time period t in Fig. 7. Then, one of the outgoing arcs, i.e., $a(n, m_1), a(n, m_2)$, and $a(n, m_3)$, or the self-loop arc $a(n, n)$ must be active at time period $t+1$. We develop ramping rate inequalities for these two scenarios separately. Before that, we introduce two definitions for ease of exposition later. First, we define $\mathcal{C}_{\to m}$ to represent the set of configurations which can transit to Configuration m. For instance, in Fig. 6, $\mathcal{C}_{\to m} = \{n_1, n_2, n_3, m\}$. Second, we define $\mathcal{C}_{n\to}$ to represent the set of configurations to which Configuration n can transit. For instance, in Fig. 7, $\mathcal{C}_{n\to} = \{m_1, m_2, m_3, n\}$.

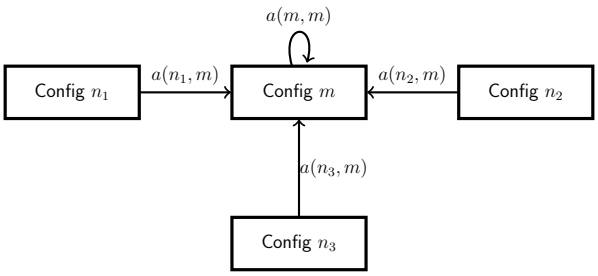

Figure 6: State Transition Graph for Configuration m

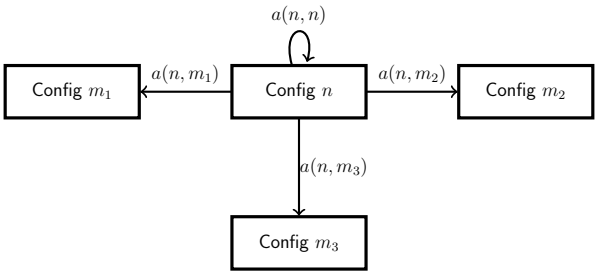

Figure 7: State Transition Graph for Configuration n

For the first scenario as shown in Fig. 6, we propose the following two strong valid inequalities.

Proposition 6. *The inequalities*

$$p_{t+1}^{m} - \sum_{n\in\mathcal{C}_{\to m}} p_t^n \le \sum_{n\in\mathcal{C}_{\to m}} RU^{a(n,m)} z_{t+1}^{a(n,m)} - \sum_{n\in\mathcal{C}_{\to m}} \underline{P}_n \left(\left(\sum_{a\in(\mathcal{A}_n^{in}\bigcup\mathcal{A}_n^{sl})} z_t^a \right) - z_{t+1}^{a(n,m)} \right), \forall m \in \mathcal{C}, \forall t, \tag{38}$$

$$\sum_{n\in\mathcal{C}_{\to m}} p_t^n - p_{t+1}^{m} \le \sum_{n\in\mathcal{C}_{\to m}} RD^{a(n,m)} z_{t+1}^{a(n,m)} + \sum_{n\in\mathcal{C}_{\to m}} \bar{P}_n \left(\left(\sum_{a\in(\mathcal{A}_n^{in}\bigcup\mathcal{A}_n^{sl})} z_t^a \right) - z_{t+1}^{a(n,m)} \right), \forall m \in \mathcal{C}, \forall t, \tag{39}$$

are valid for conv($\mathcal{Q}$). Furthermore, inequality (38) (resp. (39)) is facet-defining for the projection of polytope conv($\mathcal{Q}$) onto $\mathcal{S} = \{z_t^a, z_{t+1}^a, p_t^n, p_{t+1}^n,\ \forall a \in \mathcal{A}, \forall n \in \mathcal{C}\}$ *when* $\underline{P}_m \le \underline{P}_n + RU^{a(n,m)} < \bar{P}_m$ *(resp.* $\underline{P}_n \le \underline{P}_m + RD^{a(n,m)} < \bar{P}_n$*),* $\forall n \in \mathcal{C}_{\to m}$*, where* $\mathcal{S}$ *consists of all the variables describing inequality (38) (resp. (39)).*

Proof. First, we show the validity of ramping up inequalities (38) by discussing three possible cases as follows:

Case 1: the combined-cycle unit works on Configuration m at time period $t+1$. In this case one of the incoming arcs or the self-loop arc of Configuration m is active at time period $t+1$. For instance, in Fig. 6, one of the arcs in $\{a(n_1,m), a(n_2,m), a(n_3,m), a(m,m)\}$ is active at time period $t+1$. Suppose the combined-cycle unit works on Configuration $\bar{n}$ at time period t, where $\bar{n} \in \mathcal{C}_{\to m}$. Consequently, arc $a(\bar{n},m)$ is active at time period $t+1$. In this case, we have $z_{t+1}^{a(\bar{n},m)} = 1$, $z_{t+1}^{a(\hat{n},m)} = 0$, $\sum_{a\in(\mathcal{A}_{\bar{n}}^{\text{in}}\bigcup\mathcal{A}_{\bar{n}}^{\text{sl}})} z_t^a = 1$, and $\sum_{a\in(\mathcal{A}_{\hat{n}}^{\text{in}}\bigcup\mathcal{A}_{\hat{n}}^{\text{sl}})} z_t^a = 0$, for any $\hat{n} \in \mathcal{C}_{\to m} \setminus \{\bar{n}\}$. It follows that inequalities (38) convert to $p_{t+1}^m - p_t^{\bar{n}} \le \text{RU}^{a(\bar{n},m)}$, which is valid due to constraints (11).

Case 2: the combined-cycle unit does not work on Configuration m at time period $t+1$. However, the combined-cycle unit works on Configuration $\bar{n}$ at time period t, where $\bar{n} \in \mathcal{C}_{\to m}$. In this case, all of the incoming arcs and the self-loop arc of Configuration m are not active at time period $t+1$, which means $z_{t+1}^{a(n,m)} = 0, \forall n \in \mathcal{C}_{\to m}$. In addition, we have $\sum_{a\in(\mathcal{A}_{\bar{n}}^{\text{in}}\bigcup\mathcal{A}_{\bar{n}}^{\text{sl}})} z_t^a = 1$ and $\sum_{a\in(\mathcal{A}_{\hat{n}}^{\text{in}}\bigcup\mathcal{A}_{\hat{n}}^{\text{sl}})} z_t^a = 0$, for any $\hat{n} \in \mathcal{C}_{\to m} \setminus \{\bar{n}\}$. Then, inequalities (38) reduce to $-p_t^{\bar{n}} \le -\underline{P}_{\bar{n}}$, which is valid because of constraints (10).

Case 3: the combined-cycle unit does not work on Configuration m at time period $t+1$. Meanwhile, it does not work on any configuration in set $\mathcal{C}_{\to m}$ at time period t. In this case, all decision variables become zero in inequalities (38). Both the left and right sides of (38) will be equal to zero.

Similar analyses can be applied to inequalities (39) and thus are omitted here. Next, we show inequalities (38) and (39) are facet-defining in Appendix A.2. □

For the scenario captured in Fig. 7, we develop strong valid inequalities (40) and (41) as follows.

Proposition 7. *The inequalities*

$$\sum_{m\in\mathcal{C}_{n\rightarrow}} p^m_{t+1} - p^n_t \leq \sum_{m\in\mathcal{C}_{n\rightarrow}} RU^{a(n,m)} z^{a(n,m)}_{t+1} + \sum_{m\in\mathcal{C}_{n\rightarrow}} \bar{P}_m \left(\Big(\sum_{a\in(\mathcal{A}^{in}_m \bigcup \mathcal{A}^{sl}_m)} z^a_{t+1} \Big) - z^{a(n,m)}_{t+1} \right), \forall n \in \mathcal{C}, \forall t, \tag{40}$$

$$p^n_t - \sum_{m\in\mathcal{C}_{n\rightarrow}} p^m_{t+1} \leq \sum_{m\in\mathcal{C}_{n\rightarrow}} RD^{a(n,m)} z^{a(n,m)}_{t+1} - \sum_{m\in\mathcal{C}_{n\rightarrow}} \underline{P}_m \left(\Big(\sum_{a\in(\mathcal{A}^{in}_m \bigcup \mathcal{A}^{sl}_m)} z^a_{t+1} \Big) - z^{a(n,m)}_{t+1} \right), \forall n \in \mathcal{C}, \forall t, \tag{41}$$

are valid for conv($\mathcal{Q}$). Furthermore, inequality (40) (resp. (41)) is facet-defining for the projection of polytope conv($\mathcal{Q}$) onto set $\mathcal{S} = \{z^a_t, z^a_{t+1}, p^n_t, p^n_{t+1},\ \forall a \in \mathcal{A}, \forall n \in \mathcal{C}\}$ when $\underline{P}_m \leq \underline{P}_n + RU^{a(n,m)} < \bar{P}_m$ (resp. $\underline{P}_n \leq \underline{P}_m + RD^{a(n,m)} < \bar{P}_n$), $\forall m \in \mathcal{C}_{n\rightarrow}$, where $\mathcal{S}$ consists of all the variables describing inequality (40) (resp. (41)).

Proof. In order to verify the validity of inequalities (40), we analyze the following three possible cases, while a similar procedure can be applied to verify the validity of inequalities (41).

Case 1: the combined-cycle unit works on Configuration n at time period t and on one of the configurations (denoted by $\bar{m}$) in $\mathcal{C}_{n\rightarrow}$ at time period $t+1$. In this case, we have $z^{a(n,\bar{m})}_{t+1} = 1, z^{a(n,\hat{m})}_{t+1} = 0, \sum_{a\in(\mathcal{A}^{\text{in}}_{\bar{m}} \bigcup \mathcal{A}^{\text{sl}}_{\bar{m}})} z^a_{t+1} = 1$, and $\sum_{a\in(\mathcal{A}^{\text{in}}_{\hat{m}} \bigcup \mathcal{A}^{\text{sl}}_{\hat{m}})} z^a_{t+1} = 0$, for any $\hat{m} \in \mathcal{C}_{n\rightarrow} \setminus \{\bar{m}\}$. Then inequalities (40) convert to $p^{\bar{m}}_{t+1} - p^n_t \leq \text{RU}^{a(n,\bar{m})}$, which is valid due to constraints (11).

Case 2: the combined-cycle unit does not work on Configuration n at time period t. However, it works on one of the configurations (denoted by $\bar{m}$) in $\mathcal{C}_{n\rightarrow}$ at time period $t+1$. In this case, we have $z^{a(n,\bar{m})}_{t+1} = 0, z^{a(n,\hat{m})}_{t+1} = 0, \sum_{a\in(\mathcal{A}^{\text{in}}_{\bar{m}} \bigcup \mathcal{A}^{\text{sl}}_{\bar{m}})} z^a_{t+1} = 1$, and $\sum_{a\in(\mathcal{A}^{\text{in}}_{\hat{m}} \bigcup \mathcal{A}^{\text{sl}}_{\hat{m}})} z^a_{t+1} = 0$, for any $\hat{m} \in \mathcal{C}_{n\rightarrow} \setminus \{\bar{m}\}$. Then inequalities (40) convert to $p^{\bar{m}}_{t+1} \leq \bar{P}_{\bar{m}}$, which is valid due to constraints (10).

Case 3: the combined-cycle unit neither works on Configuration n at time period t nor works on any configuration in $\mathcal{C}_{n\rightarrow}$ at time period $t+1$. In this case, all decision variables in inequalities (40) take zeros.

Finally, since the facet-defining proofs are similar with those in Appendices A.1 and A.2, we omitted them here. □

4 Computational Results

In this section, we test the performance of our strengthened edge-based formulation on a modified IEEE 118-bus power system [1] by solving unit commitment (UC) problems with both traditional

thermal units and combined-cycle units. The complete UC formulation is provided in Appendix B.1, where the objective is to minimize the total cost including the start-up/shut-down and generation costs for operating both traditional thermal units and combined-cycle units. We first introduce the basic settings in Subsection 4.1, and then provide the computational results in solving two groups of instances in Subsections 4.2 and 4.3, respectively.

4.1 Basic Settings

We study two UC problems, i.e., one-day and two-day UC problems, with each time interval being half an hour, thereby leading to 48 and 96 time intervals in each problem, respectively. For each problem, we generate a set of instances with different load profiles based on the nominal load profile in [1]. For each instance, we compare the following five formulations:

1) "EBF", the edge-based formulation (EBF) proposed in [12];
2) "TEBF", the edge-based formulation with min-up/-down time constraints (7) and (8) replaced by tighter min-up/-down time constraints (17) and (32), respectively;
3) "REBF", the edge-based formulation with the ramping constraints (11) and (12) replaced by tighter ramping constraints (34) - (41);
4) "SEBF", our strengthened edge-based formulation in which both min-up/-down time and ramping constraints are replaced [i.e., (7) and (8) are replaced by (17) and (32), and (11) and (12) are replaced by (34) - (41)] and this is the final formulation we proposed in this paper;
5) "TCBF", the tight and compact configuration-based formulation proposed in [20], which is a strengthened configuration-based formulation in the literature.

Note here that the EBF, TEBF, and REBF models are considered benchmarks so as to show the strength of our proposed tighter constraints and strong valid inequalities in the SEBF model, and the TCBF model is considered the benchmark from the literature.

In the test system, there are 54 traditional thermal units and 12 combined-cycle units. We test this system in Subsection 4.2, and then increase the number of combined-cycle units and report the corresponding results in Subsection 4.3. All instances are solved by CPLEX 12.8 at Intel(R) Core(TM) i7-4500U 1.8GHz with 8G memory. The time limit was set at 3600 seconds per run and default CPLEX settings are applied. Note that the default optimality gap is 0.01%.

4.2 Standard Instances

For each problem, i.e., one-day and two-day UC problems, we randomly generate ten instances by following the method described in [12].

Table 2: Integrality Gap ($\times 10^{-4}$)

Case		EBF	TEBF	REBF	SEBF	TCBF
One-day	1	7.1	7.0	6.7	4.2	3.9
	2	7.1	7.1	6.7	4.1	4.5
	3	6.7	6.7	6.5	3.8	3.7
	4	7.0	7.0	6.4	3.9	3.9
	5	7.1	6.9	6.6	4.1	4.0
	6	7.3	7.2	6.8	4.3	4.0
	7	7.1	7.1	6.9	4.2	4.1
	8	7.1	7.0	6.5	4.0	3.8
	9	6.8	6.8	6.7	3.9	3.8
	10	7.0	6.9	6.7	4.0	4.4
Two-day	1	5.9	5.9	5.8	3.9	4.6
	2	6.3	6.2	5.9	4.3	4.5
	3	5.1	5.1	4.8	3.0	3.6
	4	5.6	5.6	5.1	3.6	3.8
	5	5.7	5.6	5.3	3.7	3.7
	6	4.9	4.8	4.7	2.9	3.4
	7	5.2	5.1	5.1	3.2	3.5
	8	5.5	5.5	5.2	3.5	3.6
	9	5.4	5.3	4.8	3.3	3.9
	10	6.2	6.1	5.7	4.1	4.5

We first show the effectiveness of our proposed strengthened formulation in tightening the LP relaxation of the original formulation by reporting the integrality gap information in Table 2. The integrality gap is defined as

$$\text{Integrality Gap} = \frac{\text{C}_{\text{MILP}} - \text{C}_{\text{LP}}}{\text{C}_{\text{MILP}}},$$

where C_{MILP} represents the objective value corresponding to the best integer solution obtained from all models and C_{LP} represents the LP relaxation objective value. Note here that when measuring the objective value of the LP relaxation of a mixed-integer linear program (i.e., the LP relaxation objective value), we first relax all the integer variables to be continuous and then solve the relaxed model using CPLEX as an LP solver. From Table 2, we can observe that for each instance the SEBF model provides the smallest integrality gap as compared to the EBF, TEBF, and REBF models, which means the SEBF model is tighter than them and accordingly verifies the theoretical results in Section 3. In addition, we can observe that the SEBF model induces similar integrality gaps with that of the TCBF model. Note here that as described in Section 1, TCBF is different from SEBF and it does not capture the min-up/-down time requirements of each turbine.

Next, we report the computational performances for all five models in Table 3. The column labelled "Computational Time (secs)" indicates how much time CPLEX takes to solve each instance.

Table 3: Computational Performance

Case		Computational Time (secs) (Terminal Gap($\times 10^{-4}$))					Number of Nodes				
		EBF	TEBF	REBF	SEBF	TCBF	EBF	TEBF	REBF	SEBF	TCBF
One-day	1	764.7	521.8	272.6	188.9	119.9	2811	1351	28	45	0
	2	447.1	561.2	306.0	303.9	125.0	1284	3059	0	26	21
	3	642	671.0	247.7	329.7	112.0	2446	3743	50	190	0
	4	602.9	989.7	342.5	238.9	128.0	1662	4870	0	45	35
	5	867.4	735.7	550.1	263.4	131.9	2633	3407	255	0	0
	6	2007.4	1678.6	295.6	313.1	104.4	11680	10126	107	107	0
	7	473.3	599.1	286.4	286.5	131.8	1497	2399	34	53	40
	8	669.1	580.9	286.9	190.3	89.9	3169	2832	0	0	0
	9	816.8	1397.9	374.0	271.1	144.9	4666	8020	196	38	46
	10	543.4	918.2	311.2	256.8	132.3	2081	3073	0	318	28
Two-day	1	*** (2.6)	*** (2.5)	*** (1.6)	1692.0	3182.2	4457	3970	1291	581	4003
	2	*** (2.5)	*** (2.8)	*** (2.6)	*** (1.4)	*** (1.1)	3434	2801	1645	2406	3232
	3	1995.2	*** (1.5)	2329.9	1650.7	2152.1	2052	3236	1031	1059	2467
	4	*** (2.0)	*** (1.9)	1919.2	1376.0	1381.3	5026	5316	745	531	1886
	5	*** (2.1)	*** (2.2)	2751.4	2572.1	3010.3	2895	3204	1785	1067	2428
	6	2782.9	2611.2	946.1	1189.9	1691.6	3368	2870	176	15	1904
	7	*** (1.4)	*** (1.4)	*** (1.1)	1924.0	1964.2	5775	4543	2425	662	1816
	8	*** (1.8)	*** (1.7)	*** (1.3)	1790.6	2158.2	3891	3323	1301	927	2376
	9	*** (2.4)	*** (2.4)	*** (1.3)	2377.9	2516.7	3316	4503	2588	3452	2391
	10	*** (2.8)	*** (2.4)	*** (2.2)	*** (2.0)	*** (1.5)	3327	5184	1444	1796	3160

When the CPLEX cannot solve the instance to optimality (i.e., reaching the optimality gap 0.01%) within the time limit (i.e., 3600 seconds), we indicate it by the label "***" and accordingly report the terminating gap, labelled "Terminal Gap($\times 10^{-4}$)". The column labelled "Number of Nodes" reports how many branch-and-bound nodes are explored before reaching the optimality or time limit. Note here that for each instance, the computational time includes the time within all the processes (such as root node preprocessing and heuristics) enforced by CPLEX. From Table 3, we can observe that our proposed tighter constraints and strong valid inequalities help reduce the computational time significantly. Meanwhile, as compared to the EBF, TEBF, and REBF models, the SEBF model leads to a much smaller number of branch-and-bound nodes for most instances.

In addition, we can observe that solving the problem becomes more difficult as the size of the instance increases (e.g., the size increases from one-day to two-day UC problems). For example, the EBF and TEBF models cannot solve most of the instances of the two-day UC problem to optimality within the time limit. By contrast, the SEBF model can solve most of the instances under the same setting. Furthermore, we notice that it is not needed to do branching in Cases 5 and 8 of the one-day UC problem for the SEBF model because CPLEX uses heuristic strategies and the cutting plane approach to find an optimal solution at the root node due to the small integrality gap. In addition, we can observe that the configuration-based formulation (i.e., TCBF) has a better

performance in solving one-day UC instances by relaxing the min-up/-down time restrictions of each turbine. However, in solving two-day UC instances, which are in larger sizes, the performance of TCBF is not as good as that of SEBF. In particular, SEBF takes less time and explores a smaller number of branch-and-bound nodes to solve most instances than TCBF does. In view of this, our proposed formulation SEBF is expected to perform better in solving the UC problems with a larger number of time intervals in practices, such as residual (or reliability) UC [13] and UC with small time granularity [2], than the TCBF model does.

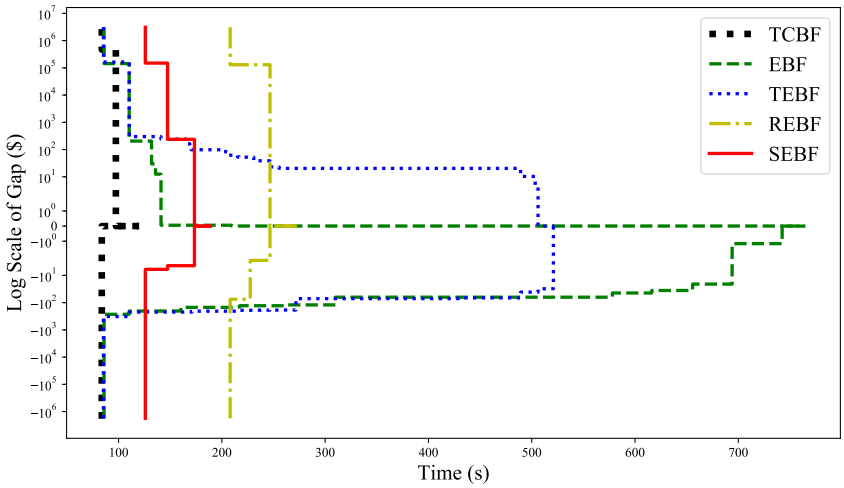

Figure 8: Convergence illustration of Case 1 in one-day UC

Finally, we report the convergence performance of the solution process to show the advantage of our strengthened edge-based formulation in accelerating the convergence process. First, we define the upper bound gap (denoted by "UBG") as the difference between the upper bound (denoted by "UB") of the model at each iteration and the optimal objective value (denoted by "OBJ") of the model, and the lower bound gap (denoted by "LBG") as the difference between the lower bound (denoted by "LB") of the model at each iteration and OBJ. Therefore, we have the following relationships:

$$\text{UBG} = \text{UB} - \text{OBJ},$$

$$\text{LBG} = \text{LB} - \text{OBJ}.$$

Then we show the convergence process in Figs. 8 and 9, where the solid (resp. dashed, dotted, and dashdotted, wide dotted) line represents the convergence of the upper bound and lower bound

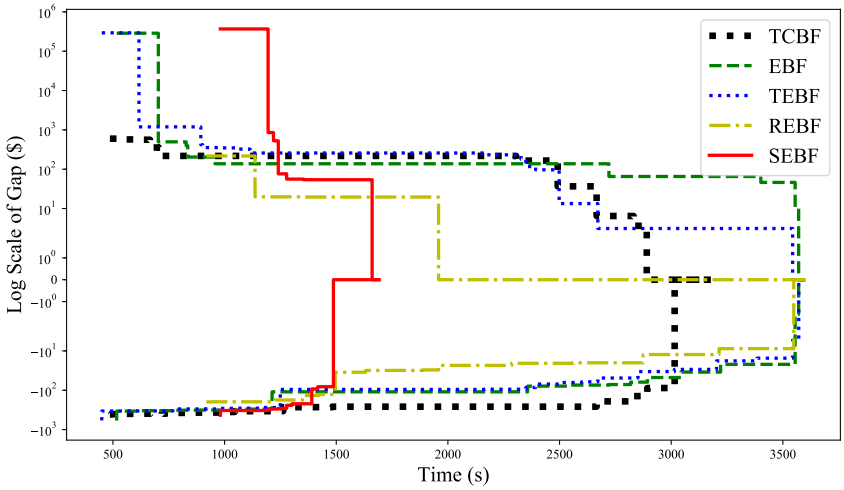

Figure 9: Convergence illustration of Case 1 in two-day UC

gaps of the SEBF (resp. EBF, TEBF, REBF, and TCBF) model. From these figures, we can observe that the SEBF model converges faster than the EBF, TEBF, and REBF models do for both one-day and two-day UC problems, and faster than the TCBF model does for two-day UC problems.

4.3 Instances with More Combined-Cycle Units

In this subsection, we increase the number of combined-cycle units to further investigate the benefits of our strengthened formulation in solving large instances with more combined-cycle units. In particular, with the number of traditional thermal units fixed at 54, we increase the number of combined-cycle units from 15 to 27, as shown in Tables 4 and 5. For each fixed number of combined-cycle units, we solve two randomly generated instances (denoted by "1" and "2" in the column labelled "Case") of a two-day UC problem with each instance corresponding to different load profiles. Similar to the results in Subsection 4.2, we provide the integrality gap information in Table 4 and the computational performance in Table 5. From the tables, we can observe that the computational performance of SEBF is better than that of any other models for most instances. In addition, the computational performance of SEBF has a very good scalability because its computational time does not increase much when the number of combined-cycle units increases in the system. Meanwhile, the SEBF model explores much less branch-and-bound nodes than other models do.

Table 4: Integrality Gap ($\times 10^{-4}$) for More Combined-Cycle Units

# CCU	Case	EBF	TEBF	REBF	SEBF	TCBF
15	1	6.3	6.3	6.1	4.3	4.5
	2	5.1	5.0	4.8	3.0	3.6
18	1	5.9	5.8	5.6	3.9	4.6
	2	5.6	5.6	5.5	3.6	3.8
21	1	5.7	5.7	5.3	3.7	3.7
	2	4.9	4.8	4.7	2.9	3.4
24	1	5.2	5.2	5.1	3.2	3.5
	2	5.5	5.4	5.4	3.5	3.6
27	1	5.4	5.4	5.9	3.3	3.9
	2	6.2	6.1	6.1	4.1	4.5

Table 5: Computational Performance for More Combined-Cycle Units

# CCU	Case	Computational Time(secs) (Terminal Gap($\times 10^{-4}$))					Number of Nodes				
		EBF	TEBF	REBF	SEBF	TCBF	EBF	TEBF	REBF	SEBF	TCBF
15	1	*** (1.8)	*** (1.1)	2032.2	997.4	1139.7	4974	7506	452	98	733
	2	*** (2.7)	*** (2.0)	*** (1.5)	1342.6	764	4996	2318	1192	21	315
18	1	*** (2.2)	*** (1.5)	*** (1.3)	1514.7	740.8	5836	5490	1350	293	835
	2	*** (2.1)	*** (1.9)	*** (1.9)	1563.6	3214.2	4635	2554	989	1475	2545
21	1	*** (2.3)	*** (2.0)	2828.7	1844.7	2767.9	3317	6069	1077	519	2504
	2	*** (1.8)	*** (1.6)	1462.9	1099.9	2012.3	6037	4324	577	0	1981
24	1	*** (3.3)	*** (3.2)	*** (1.3)	1836.8	2264.8	2019	2516	1331	1266	1536
	2	*** (3.1)	*** (2.6)	1899	1204.4	1537.3	2460	5651	631	13	1223
27	1	*** (3.4)	*** (3.0)	2266.8	1420.3	2813.9	2266	4190	0	0	2624
	2	*** (3.4)	*** (3.2)	1961.6	1647.2	2227.1	2033	1623	0	0	1472

5 Conclusions

In this paper, we focused on improving the computational performance to solve the unit commitment problems with combined-cycle units using the edge-based model, which has the advantage of exactly tracking the physical constraints over other existing models. We first derived tighter min-up/-down time and ramping rate constraints for the edge-based formulation and proved that they are tighter than the ones in the original formulation. Then, we developed several families of strong valid inequalities to further reduce the solution searching space by utilizing the physical characteristics of each individual turbine in the combined-cycle unit and the structure of its state transition graph. In addition, these strong valid inequalities can be theoretically shown to be facet-defining for the original formulation under certain mild conditions. Finally, the case studies demonstrated the effectiveness of our proposed strengthened edge-based formulation in reducing the computational time and accelerating the convergence of the solution process when solving the corresponding problems.

Acknowledgments

The authors thank the editor and the anonymous referees for their sincere suggestions, which significantly improve the quality of this paper. The authors benefit from discussion with Yonghong Chen at Midcontinent ISO and Xing Wang at Centrica. The work of K. Pan was partially supported by The Hong Kong Polytechnic University under grant G-YBUD.

References

[1] IEEE 118-bus system. https://sites.google.com/site/leifanee/dataset/, 2016.

[2] Day-ahead market enhancements. http://www.caiso.com/informed/Pages/StakeholderProcesses/Day-AheadMarketEnhancements.aspx, 2018.

[3] Agora Energiewende and Sandbag. The European power sector in 2017. *State of Affairs and Review of Current Developments*, https://sandbag.org.uk/wp-content/uploads/2018/01/EU-power-sector-report-2017.pdf, 2018.

[4] G. Anders. Commitment techniques for combined cycle generating units. *Kinectrics Inc, Toronto, Canada, CEATI Report*, (T053700-31):3, 2005.

[5] J. M. Arroyo and A. J. Conejo. Optimal response of a thermal unit to an electricity spot market. *IEEE Transactions Power Systems*, 15(3):1098–1104, 2000.

[6] CAISO. Commitment Cost Enhancements Phase 3. https://www.caiso.com/informed/Pages/StakeholderProcesses/CommitmentCostEnhancementsPhase3.aspx, 2017.

[7] M. Carrión and J. M. Arroyo. A computationally efficient mixed-integer linear formulation for the thermal unit commitment problem. *IEEE Transactions Power Systems*, 21(3):1371–1378, 2006.

[8] Y. Chen, X. Wang, and Q. Wang. Overcoming computational challenges on large scale security constrained unit commitment (SCUC) problems. http://www.ferc.gov/CalendarFiles/20140623080505-M1%20-%201%20-%20FERC2014_Chen_M1_06172014.pdf, 2014.

[9] P. Damcı-Kurt, S. Küçükyavuz, D. Rajan, and A. Atamtürk. A polyhedral study of production ramping. *Mathematical Programming*, 158(1-2):175–205, 2016.

[10] C. Dang and M. Li. A floating-point genetic algorithm for solving the unit commitment problem. *European Journal of Operational Research*, 181(3):1370–1395, 2007.

[11] L. Fan. *Bidding strategies and reformulation techniques for gas turbines under deregulated electricity markets*. PhD thesis, University of Florida, 2015.

[12] L. Fan and Y. Guan. An edge-based formulation for combined-cycle units. *IEEE Transactions Power Systems*, 31(3):1809–1819, 2016.

[13] FERC. Staff analysis of operator-initiated commitments in RTO and ISO markets. https://www.ferc.gov/legal/staff-reports/2014/AD14-14-operator-actions.pdf, 2014.

[14] H. Hui, C.-N. Yu, F. Gao, and R. Surendran. Combined cycle resource scheduling in ERCOT nodal market. In *Proc. of 2011 IEEE Power and Energy Society General Meeting*, pages 1–8.

[15] R. A. Jabr. Tight polyhedral approximation for mixed-integer linear programming unit commitment formulations. *IET Generation Transmission & Distribution*, 6(11):1104–1111, 2012.

[16] R. Jiang, M. Zhang, G. Li, and Y. Guan. Two-stage network constrained robust unit commitment problem. *European Journal of Operational Research*, 234(3):751–762, 2014.

[17] C. Liu, M. Shahidehpour, Z. Li, and M. Fotuhi-Firuzabad. Component and mode models for the short-term scheduling of combined-cycle units. *IEEE Transactions Power Systems*, 24(2):976–990, 2009.

[18] B. Lu and M. Shahidehpour. Short-term scheduling of combined cycle units. *IEEE Transactions Power Systems*, 19(3):1616–1625, 2004.

[19] MISO. Generation Portfolio Analysis. http://www.misomtep.org/generation-portfolio-analysis/, 2016.

[20] G. Morales-España, C. M. Correa-Posada, and A. Ramos. Tight and compact MIP formulation of configuration-based combined-cycle units. *IEEE Transactions Power Systems*, 31(2):1350–1359, 2016.

[21] G. Morales-España, J. M. Latorre, and A. Ramos. Tight and compact MILP formulation for the thermal unit commitment problem. *IEEE Transactions Power Systems*, 28(4):4897–4908, 2013.

[22] J. Ostrowski, M. F. Anjos, and A. Vannelli. Tight mixed integer linear programming formulations for the unit commitment problem. *IEEE Transactions Power Systems*, 27(1):39–46, 2012.

[23] K. Pan and Y. Guan. A polyhedral study of the integrated minimum-up/-down time and ramping polytope. *arXiv preprint arXiv:1604.02184*, 2016.

[24] K. Pan, Y. Guan, J.-P. Watson, and J. Wang. Strengthened MILP formulation for certain gas turbine unit commitment problems. *IEEE Transactions on Power Systems*, 31(2):1440–1448, 2016.

[25] A. Papavasiliou, Y. He, and A. Svoboda. Self-commitment of combined cycle units under electricity price uncertainty. *IEEE Transactions Power Systems*, 30(4):1690–1701, 2015.

[26] A. B. Philpott, M. Craddock, and H. Waterer. Hydro-electric unit commitment subject to uncertain demand. *European Journal of Operational Research*, 125(2):410–424, 2000.

[27] D. Rajan and S. Takriti. Minimum up/down polytopes of the unit commitment problem with start-up costs. *IBM Research Report*, 2005.

[28] A. Rong, H. Hakonen, and R. Lahdelma. A variant of the dynamic programming algorithm for unit commitment of combined heat and power systems. *European Journal of Operational Research*, 190(3):741–755, 2008.

[29] A. Rong, R. Lahdelma, and M. Grunow. An improved unit decommitment algorithm for combined heat and power systems. *European Journal of Operational Research*, 195(2):552–562, 2009.

[30] S. Takriti, B. Krasenbrink, and L. S.-Y. Wu. Incorporating fuel constraints and electricity spot prices into the stochastic unit commitment problem. *Operations Research*, 48(2):268–280, 2000.

[31] M. Tamayo, X. Yu, X. Wang, and J. Zhang. Configuration based combined cycle model in market resource commitment. In *Proc. of 2013 IEEE Power and Energy Society General Meeting*, pages 1–5.

[32] Q. Wang, Y. Guan, and J. Wang. A chance-constrained two-stage stochastic program for unit commitment with uncertain wind power output. *IEEE Transactions on Power Systems*, 27(1):206–215, 2012.

[33] L. A. Wolsey and G. L. Nemhauser. *Integer and Combinatorial Optimization*. John Wiley & Sons, 2014.

Appendix A Proofs for Strong Valid Inequalities

A.1 Facet-defining Proofs for Inequalities (36) and (37)

Proof. For each $a(n,m) \in \mathcal{A}$ at $t+1$, we show inequality (36) is facet-defining for the projection of polytope conv($\mathcal{Q}$) onto $\mathcal{S} = \{z_t^a, z_{t+1}^a, p_t^n, p_{t+1}^n,\ \forall a \in \mathcal{A}\}$ when $\underline{P}_m \le \underline{P}_n + \mathrm{RU}^{a(n,m)} < \bar{P}_m$ and $\bar{P}_m - \bar{P}_n < \mathrm{RU}^{a(n,m)},\ \forall a(n,m) \in \mathcal{A}$, where $\mathcal{S}$ consists of all the variables describing (36). As there are $2(|\mathcal{A}| + |\mathcal{C}|)$ variables in $\mathcal{S}$ and two equations in $\mathcal{Q}$, i.e., (5) and (6), the dimension of the projection of $\mathcal{Q}$ onto $\mathcal{S}$ is $2|\mathcal{A}| + |\mathcal{C}| - 1$. Thus, we generate $2|\mathcal{A}| + |\mathcal{C}| - 1$ affinely independent points as follows that satisfy (36) at equation to prove the facet-defining property. Meanwhile, we let ϵ be an arbitrarily small positive number in the following part of this paper.

As shown in Table 6, we divide these $2|\mathcal{A}| + |\mathcal{C}| - 1$ points into 14 separated groups. Each row in this table represents a point satisfying (36) at equality and each column represents a variable. To better construct points regarding variable z_{t+1}^a, we divide the arc set $\mathcal{A}$ into 6 separated sets with a given arc $a(n,m)$ as shown in (42). Similarly, we divide the arc set $\mathcal{A}$ for variable z_t^a as shown in (43).

$$\begin{aligned}
&\mathcal{A} = \bar{\mathcal{A}}_1 \cup \bar{\mathcal{A}}_2 \cup \bar{\mathcal{A}}_3 \cup \bar{\mathcal{A}}_4 \cup \bar{\mathcal{A}}_5 \cup \bar{\mathcal{A}}_6, \text{ where } \bar{\mathcal{A}}_1 = \{a(n,m)\},\ \bar{\mathcal{A}}_2 = \{a(k,m), k \in \mathcal{C}_{\to m}, k \ne n\}, \\
&\bar{\mathcal{A}}_3 = \{a(n,s), s \in \mathcal{C}_{n\to}, s \ne m\},\ \bar{\mathcal{A}}_4 = \{a(k,r), \forall k \in \mathcal{C}_{\to m}, k \ne n, \forall r \in \mathcal{C}_{k\to}, r \ne m\}, \\
&\bar{\mathcal{A}}_5 = \{a(x,x), x \in \mathcal{C}, x \ne n, x \ne k\}, \text{ and } \bar{\mathcal{A}}_6 = \{a(x,y), \forall y \in \mathcal{C}_{x\to}, x \ne n, x \ne k, y \ne x\}.
\end{aligned} \tag{42}$$

$$\begin{aligned}
&\mathcal{A} = \tilde{\mathcal{A}}_1 \cup \tilde{\mathcal{A}}_2 \cup \tilde{\mathcal{A}}_3 \cup \tilde{\mathcal{A}}_4 \cup \tilde{\mathcal{A}}_5 \cup \tilde{\mathcal{A}}_6, \text{ where } \tilde{\mathcal{A}}_1 = \{a(n,n)\}, \tilde{\mathcal{A}}_2 = \{a(u,n), u \in \mathcal{C}_{\to n}, u \ne n\} \\
&\tilde{\mathcal{A}}_3 = \{a(k,k), k \in \mathcal{C}_{\to m}, k \ne n\},\ \tilde{\mathcal{A}}_4 = \{a(v,k), k \in \mathcal{C}_{\to m}, k \ne n, v \ne k, v \in \mathcal{C}_{\to k}\}, \\
&\tilde{\mathcal{A}}_5 = \{a(x,x), x \in \mathcal{C}, x \ne n, x \ne k\}, \text{ and } \tilde{\mathcal{A}}_6 = \{a(w,x), w \in \mathcal{C}_{\to x}, w \ne x, x \ne n, x \ne k\}.
\end{aligned} \tag{43}$$

In Table 6, I represents the identity matrix and E represents the vector with 1 at each component. In addition, E_1 represents the vector with 1 at the first component and 0 at others. For a given arc $a(n,m)$, we construct these $2|\mathcal{A}| + |\mathcal{C}| - 1$ points as follows.

In Group 1, we construct one point based on the arc $a(n,m)$ by letting $z_{t+1}^{a(n,m)} = 1, z_t^{a(n,n)} = 1, p_{t+1}^m = \underline{P}_n + \mathrm{RU}^{a(n,m)}, p_t = \underline{P}_n$. In Group 2, we construct $|\mathcal{C}_{\to m}| - 1$ points based on the incoming arcs of Configuration m except the arc $a(n,m)$ (i.e. $\bar{\mathcal{A}}_2$) by letting $z_{t+1}^{a(k,m)} = 1, z_t^{a(k,k)} = 1, p_{t+1}^m = \bar{P}^m, p_t^k = \bar{P}^m - \mathrm{RU}^{a(k,m)}$ for each $k \in \mathcal{C}_{\to m}, k \ne m$. In Group 3, we let $z_{t+1}^{a(n,s)} =$

$1, z_t^{a(n,n)} = 1, p_{t+1}^s = \underline{P}_n + \mathrm{RU}^{a(n,s)}, p_t^n = \underline{P}_n$ for each outgoing arc of Configuration n except arc $a(n,m)$(i.e. $\{\forall a \in \bar{\mathcal{A}}_3\}$), where $|\mathcal{C}_{n\rightarrow}| - 1$ points are generated. In Group 4, we study the outgoing arcs of Configuration k, which can transit to Configuration m except configuration n as shown in $\bar{\mathcal{A}}_4$. Notice that arcs $a(k,m)$ are not in the set $\bar{\mathcal{A}}_4$. Then, we generate $\sum_{k\in\mathcal{C}_{\rightarrow m}, k\neq n}(|\mathcal{C}_{k\rightarrow}| - 1)$ (i.e. $|\bar{\mathcal{A}}_4|$) points by letting $z_{t+1}^{a(k,r)} = 1, z_t^{a(k,k)} = 1, p_{t+1}^r = \underline{P}_k + \mathrm{RU}^{a(k,r)}, p_t^k = \underline{P}_k$. In Group 5, we focus on the self-looping arcs for each configuration except the configurations which can transit to Configuration m (i.e. $\bar{\mathcal{A}}_5$). Accordingly, $|\mathcal{C}| - |\mathcal{C}_{\rightarrow m}|$ points are constructed by letting $z_{t+1}^{a(x,x)} = 1, z_t^{a(x,x)} = 1, p_{t+1}^x = \underline{P}_x + \mathrm{RU}^{a(x,x)}, p_t^x = \underline{P}_x$. In Group 6, we study the arcs in $\bar{\mathcal{A}}_6$. $|\mathcal{A}| - |\mathcal{C}| + 1 - \sum_{k\in\mathcal{C}_{\rightarrow m}, k\neq n}(|\mathcal{C}_{k\rightarrow}| - 1) - |\mathcal{C}_{n\rightarrow}|$ points are generated by letting $z_{t+1}^{a(x,y)} = 1, z_t^{a(x,x)} = 1, p_{t+1}^y = \underline{P}_x + \mathrm{RU}^{a(x,y)}, p_t^x = \underline{P}_x$. From Group 1 to Group 6, we generated $|\mathcal{A}|$ points in total.

In Group 7, we construct one point similar to the point in Group 1 by letting $z_{t+1}^{a(n,m)} = 1, z_t^{a(n,n)} = 1, p_{t+1}^m = \underline{P}_n + \mathrm{RU}^{a(n,m)} + \epsilon, p_t = \underline{P}_n + \epsilon$. In Group 8, we study the incoming arcs of Configuration n except the arc $a(n,n)$. $|\mathcal{C}_{\rightarrow n}| - 1$ points are constructed by letting $z_{t+1}^{a(n,m)} = 1, z_t^{a(u,n)} = 1, p_{t+1}^m = \underline{P}_n + \mathrm{RU}^{a(n,m)}, p_t = \underline{P}_n$. In Group 9, we construct $|\mathcal{C}_{\rightarrow m}| - 1$ points by using the points in Group 2 as $z_{t+1}^{a(k,m)} = 1, z_t^{a(k,k)} = 1, p_{t+1}^m = \bar{P}^m, p_t^k = \bar{P}^m - \mathrm{RU}^{a(k,m)} + \epsilon$. In Group 10, we continue to study some configuration k which can transit to Configuration m. Here, we don't include Configuration n and the self-looping arcs for Configuration k. We construct $\sum_{k\in\mathcal{C}_{\rightarrow m}, k\neq n}(|\mathcal{C}_{\rightarrow k}| - 1)$ points by letting $z_{t+1}^{a(k,m)} = 1, z_t^{a(v,k)} = 1, p_{t+1}^m = \bar{P}_m, p_t^k = \bar{P}_m - \mathrm{RU}^{a(k,m)}$. In Group 11, we construct $|\mathcal{C}| - |\mathcal{C}_{\rightarrow m}|$ points similar to those in Group 5 by letting $z_{t+1}^{a(x,x)} = 1, z_t^{a(x,x)} = 1, p_{t+1}^x = \underline{P}_x + \mathrm{RU}^{a(x,x)} + \epsilon, p_t^x = \underline{P}_x + \epsilon$. In Group 12, we study the arcs in $\tilde{\mathcal{A}}_6$. We construct $|\mathcal{A}| - |\mathcal{C}| + 1 - \sum_{k\in\mathcal{C}_{\rightarrow m}, k\neq n}(|\mathcal{C}_{\rightarrow k}| - 1) - |\mathcal{C}_{\rightarrow n}|$ points by letting $z_{t+1}^{a(x,x)} = 1, z_t^{a(x,x)} = 1, p_{t+1}^x = \underline{P}_x + \mathrm{RU}^{a(x,x)}, p_t^x = \underline{P}_x$. From Group 7 - 12, we generate $|\mathcal{A}|$ points in total.

Now, we construct the last two group of points. In Group 13, we construct $|\mathcal{C}| - |\mathcal{C}_{\rightarrow m}|$ points by letting $z_{t+1}^{a(x,x)} = 1, z_t^{a(m_0,x)} = 1, p_{t+1}^x = \underline{P}_x + \mathrm{RU}^{a(x,x)} + \epsilon, p_t^x = \underline{P}_x + \epsilon$. In Group 14, we construct $|\mathcal{C}_{\rightarrow m}| - 1$ points by letting $z_{t+1}^{a(k,m)} = 1, z_t^{a(v,k)} = 1, p_{t+1}^m = \bar{P}_m, p_t^k = \bar{P}_m - \mathrm{RU}^{a(k,m)} + \epsilon$.

In summary, we have $2|\mathcal{A}| + |\mathcal{C}| - 1$ affinely independent points satisfying (36) at equality. Similar process can be applied to show that for each $a(n,m) \in \mathcal{A}$ at $t+1$, inequality (37) is facet-defining for the projection of polytope conv($\mathcal{Q}$) onto set $\mathcal{S} = \{z_t^a, z_{t+1}^a, p_t^n, p_{t+1}^n, \ \forall a \in \mathcal{A}\}$,

Table 6: $2|\mathcal{A}| + |\mathcal{C}| - 1$ Affinely Independent Points For Inequality (36)

# Point	$z^a_{t+1}, \forall a \in \mathcal{A}$						$z^a_t, \forall a \in \mathcal{A}$						$p^c_{t+1}, \forall c \in \mathcal{C}$	$p^c_t, \forall c \in \mathcal{C}$
	$a(n,m)$	$a(k,m)$ $k \in \mathcal{C}_{\to m}$ $k \neq n$	$a(n,s)$ $s \in \mathcal{C}_{n\to}$ $s \neq m$	$a(k,r)$ $\forall k \in \mathcal{C}_{\to m}$ $k \neq n$ $\forall r \in \mathcal{C}_{k\to}, r \neq m$	$a(x,x)$ $x \in \mathcal{C}$ $x \neq n$ $x \neq k$	$a(x,y)$ $\forall y \in \mathcal{C}_{x\to}$ $x \neq n, x \neq k$ $y \neq x$	$a(n,n)$	$a(u,n)$ $u \in \mathcal{C}_{\to n}$ $u \neq n$	$a(k,k)$ $k \in \mathcal{C}_{\to m}$ $k \neq n$	$a(v,k)$ $k \in \mathcal{C}_{\to m}$ $k \neq n, v \neq k$ $v \in \mathcal{C}_{\to k}$	$a(x,x)$ $x \in \mathcal{C}$ $x \neq n$ $x \neq k$	$a(w,x)$ $w \in \mathcal{C}_{\to x}$ $w \neq x$ $x \neq n, x \neq k$		
1	1	0	0	0	0	0	1	0	0	0	0	0	$p^{c=m}_{t+1} = \underline{P}_n + \mathrm{RU}^{a(n,m)}$ $p^c_{t+1} = 0, \forall c \in \mathcal{C}, c \neq m$	$p^{c=n}_t = \underline{P}_n$ $p^c_t = 0, \forall c \in \mathcal{C}, c \neq n$
$\lvert\mathcal{C}_{\to m}\rvert - 1$	0	I	0	0	0	0	0	0	I	0	0	0	$p^{c=m}_{t+1} = \bar{P}_m$ $p^c_{t+1} = 0, \forall c \in \mathcal{C}, c \neq m$	$p^{c=k}_{t+1} = \bar{P}_m - \mathrm{RU}^{a(k,m)}$ $p^c_t = 0, \forall c \in \mathcal{C}, c \neq m$
$\lvert\mathcal{C}_{n\to}\rvert - 1$	0	0	I	0	0	0	E	0	0	0	0	0	$p^{c=s}_{t+1} = \underline{P}_n + \mathrm{RU}^{a(n,s)}$ $p^c_{t+1} = 0, \forall c \in \mathcal{C}, c \neq s$	$p^{c=n}_t = \underline{P}_n$ $p^c_t = 0, \forall c \in \mathcal{C}, c \neq n$
$\sum_{k \in \mathcal{C}_{\to m}, k \neq n} (\lvert\mathcal{C}_{k\to}\rvert - 1)$	0	0	0	I	0	0	0	0	E 0 0 0 ⋱ 0 0 0 E	0	0	0	$p^{c=k}_{t+1} = \underline{P}_k + \mathrm{RU}^{a(k,r)}$ $p^c_{t+1} = 0, \forall c \in \mathcal{C}, c \neq k$	$p^{c=k}_t = \underline{P}_k$ $p^c_t = 0, \forall c \in \mathcal{C}, c \neq k$
$\lvert\mathcal{C}\rvert - \lvert\mathcal{C}_{\to m}\rvert$	0	0	0	0	I	0	0	0	0	0	I	0	$p^{c=x}_{t+1} = \underline{P}_x + \mathrm{RU}^{x,x}$ $p^c_{t+1} = 0, \forall c \in \mathcal{C}, c \neq x$	$p^{c=x}_t = \underline{P}_x$ $p^c_t = 0, \forall c \in \mathcal{C}, c \neq x$
$\lvert\mathcal{A}\rvert - \lvert\mathcal{C}\rvert + 1$ $- \sum_{k \in \mathcal{C}_{\to m}, k \neq n} (\lvert\mathcal{C}_{k\to} - 1\rvert)$ $- \lvert\mathcal{C}_{n\to}\rvert$	0	0	0	0	0	I	0	0	0	0	E 0 0 0 ⋱ 0 0 0 E	0	$p^{c=y}_{t+1} = \underline{P}_x + \mathrm{RU}^{x,y}$ $p^c_{t+1} = 0, \forall c \in \mathcal{C}, c \neq y$	$p^{c=x}_t = \underline{P}_x$ $p^c_t = 0, \forall c \in \mathcal{C}, c \neq x$
1	1	0	0	0	0	0	1	0	0	0	0	0	$p^{c=m}_{t+1} = \underline{P}_n + \mathrm{RU}^{a(n,m)} + \epsilon$ $p^c_{t+1} = 0, \forall c \in \mathcal{C}, c \neq m$	$p^{c=n}_t = \underline{P}_n + \epsilon$ $p^c_t = 0, \forall c \in \mathcal{C}, c \neq n$
$\lvert\mathcal{C}_{\to n}\rvert - 1$	E	0	0	0	0	0	0	I	0	0	0	0	$p^{c=m}_{t+1} = \underline{P}_n + \mathrm{RU}^{a(n,m)}$ $p^c_{t+1} = 0, \forall c \in \mathcal{C}, c \neq m$	$p^{c=n}_t = \underline{P}_n$ $p^c_t = 0, \forall c \in \mathcal{C}, c \neq n$
$\lvert\mathcal{C}_{\to m}\rvert - 1$	0	I	0	0	0	0	0	0	I	0	0	0	$p^{c=m}_{t+1} = \bar{P}_m$ $p^c_{t+1} = 0, \forall c \in \mathcal{C}, c \neq m$	$p^{c=k}_{t+1} = \bar{P}_m - \mathrm{RU}^{a(k,m)} + \epsilon$ $p^c_t = 0, \forall c \in \mathcal{C}, c \neq k$
$\sum_{k \in \mathcal{C}_{\to m}, k \neq n} (\lvert\mathcal{C}_{\to k}\rvert - 1)$	0	E 0 0 0 ⋱ 0 0 0 E	0	0	0	0	0	0	0	I	0	0	$p^{c=m}_{t+1} = \bar{P}_m$ $p^c_{t+1} = 0, \forall c \in \mathcal{C}, c \neq m$	$p^{c=k}_{t+1} = \bar{P}_m - \mathrm{RU}^{a(k,m)}$ $p^c_t = 0, \forall c \in \mathcal{C}, c \neq k$
$\lvert\mathcal{C}\rvert - \lvert\mathcal{C}_{\to m}\rvert$	0	0	0	0	I	0	0	0	0	0	I	0	$p^{c=x}_{t+1} = \underline{P}_x + \mathrm{RU}^{a(x,x)} + \epsilon$ $p^c_{t+1} = 0, \forall c \in \mathcal{C}, c \neq x$	$p^{c=x}_t = \underline{P}_x + \epsilon$ $p^c_t = 0, \forall c \in \mathcal{C}, c \neq x$
$\lvert\mathcal{A}\rvert - \lvert\mathcal{C}\rvert + 1$ $- \sum_{k \in \mathcal{C}_{\to m}, k \neq n} (\lvert\mathcal{C}_{\to k}\rvert)$ $- \lvert\mathcal{C}_{\to n}\rvert$	0	0	0	0	E 0 0 0 ⋱ 0 0 0 E	0	0	0	0	0	0	I	$p^{c=x}_{t+1} = \underline{P}_x + \mathrm{RU}^{a(x,x)}$ $p^c_{t+1} = 0, \forall c \in \mathcal{C}, c \neq x$	$p^{c=x}_t = \underline{P}_x$ $p^c_t = 0, \forall c \in \mathcal{C}, c \neq x$
$\lvert\mathcal{C}\rvert - \lvert\mathcal{C}_{\to m}\rvert$	0	0	0	0	I	0	0	0	0	0	0	E_1 0 ⋯ 0 0 0 E_1 ⋯ 0 0 0 0 ⋱ 0 0 0 0 ⋯ E_1 0 0 0 ⋯ 0 E_1	$p^{c=x}_{t+1} = \underline{P}_x + \mathrm{RU}^{a(x,x)} + \epsilon$ $p^c_{t+1} = 0, \forall c \in \mathcal{C}, c \neq x$	$p^{c=x}_t = \underline{P}_x + \epsilon$ $p^c_t = 0, \forall c \in \mathcal{C}, c \neq x$
$\lvert\mathcal{C}_{\to m}\rvert - 1$	0	I	0	0	0	0	0	0	0	E_1 0 ⋯ 0 0 0 E_1 ⋯ 0 0 0 0 ⋱ 0 0 0 0 ⋯ E_1 0 0 0 ⋯ 0 E_1	0	0	$p^{c=m}_{t+1} = \bar{P}_m$ $p^c_{t+1} = 0, \forall c \in \mathcal{C}, c \neq m$	$p^{c=k}_t = \bar{P}_m - \mathrm{RU}^{a(k,m)} + \epsilon$ $p^c_t = 0, \forall c \in \mathcal{C}, c \neq k$

which consists of all the variables describing inequality (37), when $\underline{P}_n \leq \underline{P}_m + \mathrm{RD}^{a(n,m)} < \bar{P}_n$ and $\bar{P}_n - \bar{P}_m < \mathrm{RD}^{a(n,m)}$, $\forall a(n,m) \in \mathcal{A}$ for (37). Thus the details are omitted here. □

A.2 Facet-defining Proof for Inequality (38)

Proof. For each $m \in \mathcal{C}$ and t, we show inequality (38) is facet-defining for the projection of polytope conv($\mathcal{Q}$) onto $\mathcal{S} = \{z_t^a, z_{t+1}^a, p_t^n, p_{t+1}^n, \forall a \in \mathcal{A}, \forall n \in \mathcal{C}\}$ when $\underline{P}_m \leq \underline{P}_n + \mathrm{RU}^{a(n,m)} < \bar{P}_m$, $\forall n \in \mathcal{C}_{\to m}$, where $\mathcal{S}$ consists of all the variables describing inequality (38). As there are $2(|\mathcal{A}| + |\mathcal{C}|)$ variables in $\mathcal{S}$, $\sum_{a \in (\mathcal{A}_k^{\mathrm{in}} \bigcup \mathcal{A}_k^{\mathrm{sl}})} z_t^a = \sum_{a \in (\mathcal{A}_k^{\mathrm{out}} \bigcup \mathcal{A}_k^{\mathrm{sl}})} z_{t+1}^a, \forall k \in \mathcal{C}$, and $\sum_{a \in \mathcal{A}} z_t^a = 1$, the dimension of the projection of $\mathcal{Q}$ onto $\mathcal{S}$ is $2|\mathcal{A}| + |\mathcal{C}| - 1$. In the following, we provide $2|\mathcal{A}| + |\mathcal{C}| - 1$ affinely independent points that satisfy (38) at equality to show the property of facet-defining [33], see Table 7.

In Table 7, there are 11 groups of points in total, with each row representing one point satisfying (38) at equality and each column representing the value of each variable. Meanwhile, we let I represent an identity matrix and 0 represent a zero matrix. Note here that in order to save space, we use (m,n) to represent arc $a(m,n)$ in the header of Table 7. We generate these points in the following ways:

1. In Groups 1 - 3, we construct a lower matrix in terms of the value of z_t^a, $\forall a \in \mathcal{A}$. In particular, in Group 1, for each $k \in \mathcal{C}_{\to m}$ (totally $|\mathcal{C}_{\to m}|$ points), we let $z_t^{a(k,m)} = 1$, $z_{t+1}^{a(m,m)} = 1$, $p_t^m = \underline{P}_m$, and $p_{t+1}^m = \underline{P}_m + \mathrm{RU}^{a(m,m)}$; in Group 2, for each $s \in \mathcal{C}_{m\to}$, $s \neq m$ (totally $|\mathcal{C}_{m\to}| - 1$ points, note that we rule out $s = m$ to avoid duplication), we let $z_t^{a(m,s)} = 1$, $z_{t+1}^{a(s,s)} = 1$, and $p_t^s = p_{t+1}^s = \underline{P}_s$; in Group 3, for each remaining arcs of $\mathcal{A}$ (totally $|\mathcal{A}| - |\mathcal{C}_{\to m}| - (|\mathcal{C}_{m\to}| - 1)$ points), i.e., $a(x,y)$, we let $z_t^{a(x,y)} = 1$, $z_{t+1}^{a(y,y)} = 1$, $p_t^y = \underline{P}_y$, and $p_{t+1}^y = \underline{P}_y$. Therefore, in total we generate $|\mathcal{A}|$ points here.
2. In Groups 4 - 6, we continue to construct a lower matrix in terms of the value of z_{t+1}^a, $\forall a \in \mathcal{A}$, which together with the lower matrix generated in Groups 1 - 3 can be easily transformed to a large lower matrix through Gaussian elimination. In particular, in Group 4, for each $k \in \mathcal{C}_{\to m}$, $k \neq m$ (totally $|\mathcal{C}_{\to m}| - 1$ points, note that we rule out $k = m$ to avoid duplicating one point in group 1), we let $z_t^{a(k,k)} = 1$, $z_{t+1}^{a(k,m)} = 1$, $p_t^k = \underline{P}_k$, and $p_{t+1}^m = \underline{P}_k + \mathrm{RU}^{a(k,m)}$; in Group 5, for each $s \in \mathcal{C}_{m\to}$, $s \neq m$ (totally $|\mathcal{C}_{m\to}| - 1$ points), we let $z_t^{a(m,m)} = 1$, $z_{t+1}^{a(m,s)} = 1$, $p_t^m = \underline{P}_m$, and $p_{t+1}^s = \underline{P}_s$; in Group 6, for each remaining arcs of $\mathcal{A} \setminus \{(n,n), \forall n \in \mathcal{C}\}$ (totally

$|\mathcal{A}| - |\mathcal{C}| - (|\mathcal{C}_{\to m}| - 1) - (|\mathcal{C}_{m\to}| - 1)$ points, note that we rule out $a(n,n), \forall n \in \mathcal{C}$ to avoid duplication with Groups 1 - 3), i.e., $a(x,y)$ with $x \neq y$, we let $z_t^{a(x,x)} = 1$, $z_{t+1}^{a(x,y)} = 1$, $p_t^x = \underline{P}_x$, and $p_{t+1}^y = \underline{P}_y$. Therefore, in total we generate $|\mathcal{A}| - |\mathcal{C}|$ points here.

3. In Groups 7 - 9, we generate $|\mathcal{C}|$ points by utilizing the points in Groups 1 - 3 so that the points in these groups together with the points above can be easily transformed to a lower matrix. In particular, in Group 7 (totally one point), we choose one $\bar{k} \in \mathcal{C}_{\to m}$ (e.g., $\bar{k} = m$) and let $z_t^{a(\bar{k},m)} = 1$, $z_{t+1}^{a(m,m)} = 1$, $p_t^m = \underline{P}_m + \epsilon$, and $p_{t+1}^m = \underline{P}_m + \mathrm{RU}^{a(m,m)} + \epsilon$; in Group 8, for each $s \in \mathcal{C}_{m\to}$, $s \neq m$ (totally $|\mathcal{C}_{m\to}| - 1$ points), we let $z_t^{a(m,s)} = 1$, $z_{t+1}^{a(s,s)} = 1$, and $p_t^s = p_{t+1}^s = \underline{P}_s + \epsilon$; in Group 9, for each remaining configuration of $\mathcal{C}$ (totally $|\mathcal{C}| - 1 - (|\mathcal{C}_{m\to}| - 1)$ points), i.e., $a(x,y)$ with $y \in \mathcal{C} \setminus \{\mathcal{C}_{m\to}\}$ for some x, we let $z_t^{a(x,y)} = 1$, $z_{t+1}^{a(y,y)} = 1$, $p_t^y = \underline{P}_y + \epsilon$, and $p_{t+1}^y = \underline{P}_y + \epsilon$. Therefore, in total we generate $|\mathcal{C}|$ points here. We can easily observe that the points in Groups 7-9 together with the points in Groups 1-3 can be transformed to a lower matrix in terms of the values of z_t^a, $\forall a \in \mathcal{A}$ and p_{t+1}^n, $\forall n \in \mathcal{C}$.

4. In Groups 10 - 11, we generate $|\mathcal{C}| - 1$ points by utilizing the points in Groups 4 - 6 so that the points in these groups together with the points above can be easily transformed to a lower matrix. In particular, in Group 10, for each $k \in \mathcal{C}_{\to m}$, $k \neq m$ (totally $|\mathcal{C}_{\to m}| - 1$ points), we let $z_t^{a(k,k)} = 1$, $z_{t+1}^{a(k,m)} = 1$, $p_t^k = \underline{P}_k + \epsilon$, and $p_{t+1}^m = \underline{P}_k + \mathrm{RU}^{a(k,m)} + \epsilon$; in Group 11, for each remaining configuration of $\mathcal{C} \setminus \mathcal{C}_{\to m}$ (totally $|\mathcal{C}| - (|\mathcal{C}_{\to m}| - 1) - 1$ points), i.e., $a(x,y)$ with $x \in \mathcal{C} \setminus \mathcal{C}_{\to m}$ for some y and $x \in \{m, y\}$, we let $z_t^{a(x,x)} = 1$, $z_{t+1}^{a(x,y)} = 1$, $p_t^x = \underline{P}_x + \epsilon$, and $p_{t+1}^y = \underline{P}_y + \epsilon$. Thus, in total we generate $|\mathcal{C}| - 1$ points here. We can easily observe that the points in Groups 10-11 together with the points in Groups 4-6 can be transformed to a lower matrix in terms of the values of z_{t+1}^a, $\forall a \in \mathcal{A}$ and p_t^n, $\forall n \in \mathcal{C} \setminus \{m\}$.

In summary, it is clear that $2|\mathcal{A}| + |\mathcal{C}| - 1$ points generated above satisfy (38) at equality and can easily be transformed to a lower matrix with dimension at least $2|\mathcal{A}| + |\mathcal{C}| - 2$, which means that these points are affinely independent. Similar process can be applied to show that for each $m \in \mathcal{C}$ and t, inequality (39) is facet-defining for the projection of polytope conv($\mathcal{Q}$) onto set $\mathcal{S} = \{z_t^a, z_{t+1}^a, p_t^n, p_{t+1}^n, \ \forall a \in \mathcal{A}, \forall n \in \mathcal{C}\}$, which consists of all the variables describing inequality (39), when $\underline{P}_n \leq \underline{P}_m + \mathrm{RD}^{a(n,m)} < \bar{P}_n$, $\forall n \in \mathcal{C}_{\to m}$ for (39). Thus the details are omitted here. □

Table 7: $2|\mathcal{A}| + |\mathcal{C}| - 1$ affinely independent points for (38)

# Point	$z_t^a,\ \forall a \in \mathcal{A}$			$z_{t+1}^a,\ \forall a \in \mathcal{A}$			$p_t^n,\ \forall n \in \mathcal{C}$					$p_{t+1}^n,\ \forall n \in \mathcal{C}$				
	$(k,m), \forall k \in \mathcal{C}_{\to m}$	$(m,s), \forall s \in \mathcal{C}_{m\to}$ $s \neq m$	(x,y) $x \neq m$ $y \neq m$	$(k,m), \forall k \in \mathcal{C}_{\to m}$	$(m,s), \forall s \in \mathcal{C}_{m\to}$ $s \neq m$	(x,y) $x \neq m$ $y \neq m$	$\forall k \in \mathcal{C}_{\to m}$	m	$(m,s), \forall s \in \mathcal{C}_{m\to}$ $s \neq m$	$x \neq m$	$y \neq m$	$\forall k \in \mathcal{C}_{\to m}$	m	$(m,s), \forall s \in \mathcal{C}_{m\to}$ $s \neq m$	$x \neq m$	$y \neq m$
$\lvert\mathcal{C}_{\to m}\rvert$	I	0	0	$z_{t+1}^{a(k,m)} = 1$, if $k = m$; $0, o.w.$	0	0	0	$\underline{P}_m$ $\underline{P}_m$ $\underline{P}_m$	0	0	0	0	$\underline{P}_m + \mathrm{RU}^{a(m,m)}$ $\underline{P}_m + \mathrm{RU}^{a(m,m)}$ $\underline{P}_m + \mathrm{RU}^{a(m,m)}$	0	0	0
$\lvert\mathcal{C}_{m\to}\rvert - 1$	0	I	0	0	0	$z_{t+1}^{a(s,s)} = 1$	0	0 0 0	$\underline{P}_s$ 0 $\cdots$ 0 $\underline{P}_s$	0	0	0	0 0 0	$\underline{P}_s$ 0 $\cdots$ 0 $\underline{P}_s$	0	0
$\lvert\mathcal{A}\rvert + 1$ $-\lvert\mathcal{C}_{\to m}\rvert$ $-\lvert\mathcal{C}_{m\to}\rvert$	0	0	I	0	0	$z_{t+1}^{a(y,y)} = 1$	0	0 0 0	0	0	$\underline{P}_y$ 0 $\cdots$ 0 $\underline{P}_y$	0	0 0 0	0	0	$\underline{P}_y$ 0 $\cdots$ 0 $\underline{P}_y$
$\lvert\mathcal{C}_{\to m}\rvert - 1$	0	0	$z_t^{a(k,k)} = 1$	I $(k \neq m)$	0	0	$\underline{P}_k$ 0 $\cdots$ 0 $\underline{P}_k$	0 0 0	0	0	0	0	$\underline{P}_k + \mathrm{RU}^{a(k,m)}$ $\underline{P}_k + \mathrm{RU}^{a(k,m)}$ $\underline{P}_k + \mathrm{RU}^{a(k,m)}$	0	0	0
$\lvert\mathcal{C}_{m\to}\rvert - 1$	$z_t^{a(m,m)} = 1$	0	0	0	I	0	0	$\underline{P}_m$ $\underline{P}_m$ $\underline{P}_m$	0	0	0	0	0 0 0	$\underline{P}_s$ 0 $\cdots$ 0 $\underline{P}_s$	0	0
$\lvert\mathcal{A}\rvert - \lvert\mathcal{C}\rvert + 2 - \lvert\mathcal{C}_{\to m}\rvert - \lvert\mathcal{C}_{m\to}\rvert$	0	0	$z_t^{a(x,x)} = 1$ $x \neq y$	0	0	I	0	0 0 0	0	$\underline{P}_x$ 0 $\cdots$ 0 $\underline{P}_x$	0	0	0 0 0	0	0	$\underline{P}_y$ 0 $\cdots$ 0 $\underline{P}_y$
1	1 0 $\cdots$ 0	0 0 $\cdots$ 0	0 0 $\cdots$ 0	0 $\cdots$ 0 1	0 0 0	0 0 0	0 0	$\underline{P}_m + \epsilon$	0 0	0 0	0 0	0 0	$\underline{P}_m + \epsilon + \mathrm{RU}^{a(m,m)}$	0 0	0 0	0 0
$\lvert\mathcal{C}_{m\to}\rvert - 1$	0	I	0	0	0	$z_{t+1}^{a(s,s)} = 1$	0	0 0 0	$\underline{P}_s + \epsilon$ 0 $\cdots$ 0 $\underline{P}_s + \epsilon$	0	0	0	0 0 0	$\underline{P}_s + \epsilon$ 0 $\cdots$ 0 $\underline{P}_s + \epsilon$	0	0
$\lvert\mathcal{C}\rvert$ $\lvert\mathcal{C}_{m\to}\rvert$	0	0	I	0	0	$z_{t+1}^{a(y,y)} = 1$	0	0 0 0	0	0	$\underline{P}_y + \epsilon$ 0 $\cdots$ 0 $\underline{P}_y + \epsilon$	0	0 0 0	0	0	$\underline{P}_y + \epsilon$ 0 $\cdots$ 0 $\underline{P}_y + \epsilon$
$\lvert\mathcal{C}_{\to m}\rvert - 1$	0	0	$z_t^{a(k,k)} = 1$	I $(k \neq m)$	0	0	$\underline{P}_k + \epsilon$ 0 $\cdots$ 0 $\underline{P}_k + \epsilon$	0 0 0	0	0	0	0	$\underline{P}_k + \epsilon + \mathrm{RU}^{a(k,m)}$ $\underline{P}_k + \epsilon + \mathrm{RU}^{a(k,m)}$ $\underline{P}_k + \epsilon + \mathrm{RU}^{a(k,m)}$	0	0	0
$\lvert\mathcal{C}\rvert - \lvert\mathcal{C}_{\to m}\rvert$	0	0	$z_t^{a(x,x)} = 1$ $x \neq y$	0	0	I	0	0 0 0	0	$\underline{P}_x + \epsilon$ 0 $\cdots$ 0 $\underline{P}_x + \epsilon$	0	0	0 0 0	0	0	$\underline{P}_y + \epsilon$ 0 $\cdots$ 0 $\underline{P}_y + \epsilon$

Appendix B Notations and UC formulation

In this section, we first summarize all the notations (i.e., sets, parameters, and decision variables) for combined-cycle units and traditional thermal units in Tables 8 and 9, respectively. Then we describe the complete mathematical formulation of a unit commitment problem including both traditional thermal units and combined-cycle units in Appendix B.1.

Table 8: Notations for Combined-Cycle Units

Sets		**Parameters**	
$\mathcal{A}$	set of all the arcs	$\underline{P}_k$	minimal power output of configuration k
$\mathcal{A}_k^{\text{all}}$	set of arcs linked to configuration k	$\bar{P}_k$	maximal power output of configuration k
$\mathcal{A}_k^{\text{in}}$	set of incoming arcs of configuration k	$\bar{P}^c$	total capacity of a combined-cycle unit
$\mathcal{A}_k^{\text{out}}$	set of outgoing arcs of configuration k	RU^a	ramping up limit of arc a
$\mathcal{A}_i^{\text{on}}$	set of arcs indicating turbine i keeps online	RD^a	ramping down limit of arc a
$\mathcal{A}_i^{\text{off}}$	set of arcs indicating turbine i keeps offline	T_{mu}^i	min-up time requirement of turbine i
$\mathcal{A}_k^{\text{sl}}$	set of self-loop arcs of configuration k	T_{md}^i	min-down time requirement of turbine i
$\mathcal{A}_i^{\text{sd}}$	set of arcs indicating turbine i shuts down	$\bar{V}_1^i$	hot start-up cost for turbine i
$\mathcal{A}_i^{\text{su}}$	set of arcs indicating turbine i starts up	$\delta_{1,2}^i$	the difference between the warm and hot start-up costs for turbine i
$\mathcal{C}$	set of all the configurations	$\delta_{2,3}^i$	the difference between the cold and warm start-up costs for turbine i
$\mathcal{U}^{\text{CT}}$	set of CTs in a combined-cycle unit	$\underline{V}^i$	shut-down cost for turbine i
$\mathcal{U}^{\text{ST}}$	set of STs in a combined-cycle unit	T_{c}^i	cold start time for turbine i
$\mathcal{T}$	set of scheduling time periods	T_{w}^i	warm start time for turbine i
Decision Variables		T_{h}^i	hot start time for turbine i
z_t^a	online/offline status of arc a at time t		
p_t	generation amount of the whole combined-cycle unit at t		
p_t^k	generation amount of configuration k at t		
ϕ_t^k	generation cost of configuration k at t		
φ_t^i	start-up cost of turbine i at t		
Θ	total operating cost		

B.1 Complete UC Formulation

We let $\mathcal{U}^{\text{CC}}$ represent the set of combined-cycle units that will be considered in the unit commitment problem, and let $\mathcal{U}_b^{\text{CC}}$ represent the set of combined-cycle units at each bus $b \in \mathcal{B}$. We add superscript n to all the notations in Table 8 to indicate the corresponding sets, parameters, and decision variables for combined-cycle unit $n \in \mathcal{U}^{\text{CC}}$. Therefore, the complete unit commitment formulation including both traditional thermal units and combined-cycle units can be described as

Table 9: Notations for Traditional Thermal Units, Buses, and Transmission Lines

Sets		**Parameters**	
$\mathcal{B}$	set of buses	CU^n	start-up cost of unit n
$\mathcal{L}$	set of transmission lines	CD^n	shut-down cost of unit n
$\mathcal{U}^{\mathrm{T}}$	set of traditional thermal units	$C_{b,l}$	capacity limits of transmission line (b,l)
$\mathcal{U}_b^{\mathrm{T}}$	set of thermal units at bus b	$X_{b,l}$	Reactance of transmission line (b,l)
Decision Variables		D_t^b	generation demand at bus b at time t
x_t^n	start-up indicator for thermal unit n at time t	$\underline{P}^n$	minimum generation output of unit n
y_t^n	shut-down indicator for thermal unit n at t	$\bar{P}^n$	maximum generation output of unit n
w_t^n	on/off status indicator for thermal unit n at t	RD^n	ramping down limit of thermal unit n
p_t^n	generation amount of thermal unit n at t	RU^n	ramping up limit of thermal unit n
θ_t^b	phase angle of bus b at t	T_{md}^n	min-down time requirement for unit n
		T_{mu}^n	min-up time requirement for unit n

follows.

$$\min \quad \sum_{n\in\mathcal{U}^{\mathrm{CC}}} \Theta^n + \sum_{n\in\mathcal{U}^{\mathrm{T}}}\sum_{t\in\mathcal{T}}\Big(\mathrm{CU}^n x_t^n + \mathrm{CD}^n y_t^n + \phi_t^n(p_t^n)\Big) \tag{44}$$

$$\text{s.t.} \quad x_t^n + y_t^n \le 1,\ \forall n \in \mathcal{U}^{\mathrm{T}}, \forall t \in \mathcal{T}, \tag{45}$$

$$w_t^n - w_{t-1}^n = x_t^n - y_t^n,\ \forall n \in \mathcal{U}^{\mathrm{T}}, \forall t \in \mathcal{T}, \tag{46}$$

$$\sum_{\tau=t-T_{\mathrm{mu}}^n+1}^{t} x_\tau^n \le w_t^n,\ \forall n \in \mathcal{U}^{\mathrm{T}}, \forall t \in \{T_{\mathrm{mu}}^n, \cdots, \mathcal{T}_{\mathrm{end}}\}, \tag{47}$$

$$\sum_{\tau=t-T_{\mathrm{md}}^n+1}^{t} y_\tau^n \le 1 - w_t^n,\ \forall n \in \mathcal{U}^{\mathrm{T}}, \forall t \in \{T_{\mathrm{md}}^n, \cdots, \mathcal{T}_{\mathrm{end}}\}, \tag{48}$$

$$\underline{P}^n w_t^n \le p_t^n \le \bar{P}^n w_t^n,\ \forall n \in \mathcal{G}^{\mathrm{T}}, \forall t \in \mathcal{T}, \tag{49}$$

$$p_t^n - p_{t-1}^n \le RU^n w_{t-1}^n + \overline{RU}^n x_t^n,\ \forall n \in \mathcal{U}^{\mathrm{T}}, \forall t \in \mathcal{T}, \tag{50}$$

$$p_{t-1}^n - p_t^n \le RD^n w_t^n + \overline{RD}^n y_t^n,\ \forall n \in \mathcal{U}^{\mathrm{T}}, \forall t \in \mathcal{T}, \tag{51}$$

$$x_t^n, y_t^n, w_t^n \in \{0,1\},\ \forall n \in \mathcal{U}^{\mathrm{T}}, \forall t \in \mathcal{T},$$

$$\sum_{n\in\mathcal{U}_b^{\mathrm{T}}} p_t^n + \sum_{k\in\mathcal{U}_b^{\mathrm{CC}}} p_t^k - \mathrm{D}_t^b - \sum_{(b,l)\in\mathcal{L}} \frac{\theta_t^b - \theta_t^l}{X_{b,l}} = 0,\ \forall b \in \mathcal{B}, \forall t \in \mathcal{T}, \tag{52}$$

$$-C_{b,l} \le \frac{\theta_t^b - \theta_t^l}{X_{b,l}} \le C_{b,l},\ \forall (b,l) \in \mathcal{L}, \forall t \in \mathcal{T}, \tag{53}$$

$$(5) - (16),\ \forall n \in \mathcal{U}^{\mathrm{CC}}.$$

The objective function is to minimize the total cost including the operational cost of combined-cycle units (i.e., Θ) and that of traditional thermal units [i.e., $\sum_{t\in\mathcal{T}}\sum_{n\in\mathcal{U}^{\mathrm{T}}}(\mathrm{CU}^n x_t^n + \mathrm{CD}^n y_t^n + \phi_t^n(p_t^n))$], where the first, second, and third terms in the inner bracket represent the start-up, shut-down,

and production costs of thermal units, respectively. The production cost ($\phi_t^n(p_t^n)$) is a quadratic polynomial function of the power output p_t^n. This quadratic function is normally approximated by piecewise linear function in practice. Constraints (45) - (46) represent the relationship among the start-up binary indicator (x_t^n), shut-down binary indicator (y_t^n) and on/off status binary indicator (w_t^n) for each traditional thermal unit. Constraints (47) and (48) represents the min-up/-down time requirements for each traditional thermal unit. Constraints (49) describe the generation limits for each traditional thermal unit. Constraints (50) and (51) enforce the ramping rate limits for each traditional thermal unit. Constraints (52) represent the power balance requirement for each bus. Constraints (53) represent the transmission line limits. Constraints (5) - (16) represent all the operational constraints of the combined-cycle units, as we shown in Section 2.